








## ARTICLE

# Continuous mitotic activity of primitive hematopoietic stem cells in adult mice

Mina N.F. Morcos<sup>1</sup>, Thomas Zerjatke<sup>2</sup> , Ingmar Glauche<sup>2</sup> , Clara M. Munz<sup>1</sup>, Yan Ge<sup>1</sup>, Andreas Petzold<sup>3</sup>, Susanne Reinhardt<sup>3</sup>, Andreas Dahl<sup>3</sup>, Natasha S. Anstee<sup>4</sup> , Ruzhica Bogeska<sup>4</sup> , Michael D. Milsom<sup>4</sup>, Petter Säwén<sup>5</sup> , Haixia Wan<sup>5</sup>, David Bryder<sup>5,6</sup> , Axel Roers<sup>1</sup>, and Alexander Gerbaulet<sup>1</sup> 

**The proliferative activity of aging hematopoietic stem cells (HSCs) is controversially discussed. Inducible fluorescent histone 2B fusion protein (H2B-FP) transgenic mice are important tools for tracking the mitotic history of murine HSCs in label dilution experiments. A recent study proposed that primitive HSCs symmetrically divide only four times to then enter permanent quiescence. We observed that background fluorescence due to leaky H2B-FP expression, occurring in all H2B-FP transgenes independent of label induction, accumulated with age in HSCs with high repopulation potential. We argue that this background had been misinterpreted as stable retention of induced label. We found cell division-independent half-lives of H2B-FPs to be short, which had led to overestimation of HSC divisional activity. Our data do not support abrupt entry of HSCs into permanent quiescence or sudden loss of regeneration potential after four divisions, but show that primitive HSCs of adult mice continue to cycle rarely.**

## Introduction

The multipotent and self-renewing hematopoietic stem cells (HSCs) reside at the top of the hematopoietic hierarchy and can give rise to all blood lineages throughout the life of an individual (Eaves, 2015). Numerous studies have unambiguously demonstrated heterogeneous cell cycle activity within the HSC population (Foudi et al., 2009; Glauche et al., 2009; Morcos et al., 2017; Passegué et al., 2005; Qiu et al., 2014; Säwén et al., 2016; Takizawa et al., 2011; Wilson et al., 2008). A concept of deeply quiescent (also termed “dormant”) and actively cycling HSCs has been firmly established from experiments investigating mitotic history by means of labeled nucleotide analogues (e.g., BrdU; Kiel et al., 2007; Wilson et al., 2008) or histone 2B (H2B) fused to either enhanced green fluorescent protein (H2B-GFP) or mCherry (hereafter referred to as H2B-RFP; Foudi et al., 2009; Qiu et al., 2014; Säwén et al., 2016; Wilson et al., 2008). These labels get incorporated into chromatin (Egli et al., 2007; Kanda et al., 1998) and are homogeneously distributed to daughter cells during mitosis (Tumbar et al., 2004), which allows for the tracking of several cell divisions as well as the identification of quiescent label retaining cells. In case of the H2B-fusion proteins (H2B-FPs), labeling of HSCs is achieved with inducible tetracycline (Tet) controlled (either “Tet-on” or “Tet-off”) genetic

systems (Gossen and Bujard, 2002). Importantly, these mouse models exhibit considerable background fluorescence even in the repressed state due to leaky expression from the Tet-operon (Challen and Goodell, 2008; Foudi et al., 2009; Qiu et al., 2014; Säwén et al., 2016; Tumbar et al., 2004; Wilson et al., 2008).

A recent study (Bernitz et al., 2016) reported HSCs retaining pulsed H2B-GFP label for up to 22 mo of chase. Based on this finding, the authors proposed a model in which the most primitive HSCs that contain all long-term repopulating activity enter complete and permanent quiescence after initially undergoing four symmetric self-renewal divisions. However, neither division-independent loss by protein degradation (Waghmare et al., 2008), which even in case of slow degradation would preclude long chase periods, nor the continuous leaky background expression (Challen and Goodell, 2008) of H2B-FPs was considered in this model.

In the present study, we reevaluated H2B-FP retention. We show that in three different H2B-FP transgenic mouse strains, the most quiescent HSC subpopulation inevitably accumulates high background fluorescence in an age-dependent manner. Accordingly, long-term serial repopulation activity was enriched among cells with high background. We estimated

<sup>1</sup>Institute for Immunology, Faculty of Medicine, TU Dresden, Dresden, Germany; <sup>2</sup>Institute for Medical Informatics and Biometry, Faculty of Medicine, TU Dresden, Dresden, Germany; <sup>3</sup>DRESDEN-concept Genome Center, Center for Molecular and Cellular Bioengineering, TU Dresden, Dresden, Germany; <sup>4</sup>Division of Experimental Hematology, Deutsches Krebsforschungszentrum and Heidelberg Institute for Stem Cell Technology and Experimental Medicine, Heidelberg, Germany; <sup>5</sup>Division of Molecular Hematology, Lund University, Lund, Sweden; <sup>6</sup>Sahlgrenska Cancer Centre, Gothenburg University, Gothenburg, Sweden.

Correspondence to Alexander Gerbaulet: [alexander.gerbaulet@tu-dresden.de](mailto:alexander.gerbaulet@tu-dresden.de); Thomas Zerjatke: [thomas.zerjatke@tu-dresden.de](mailto:thomas.zerjatke@tu-dresden.de).

© 2020 Morcos et al. This article is distributed under the terms of an Attribution-Noncommercial-Share Alike-No Mirror Sites license for the first six months after the publication date (see <http://www.rupress.org/terms/>). After six months it is available under a Creative Commons License (Attribution-Noncommercial-Share Alike 4.0 International license, as described at <https://creativecommons.org/licenses/by-nc-sa/4.0/>).

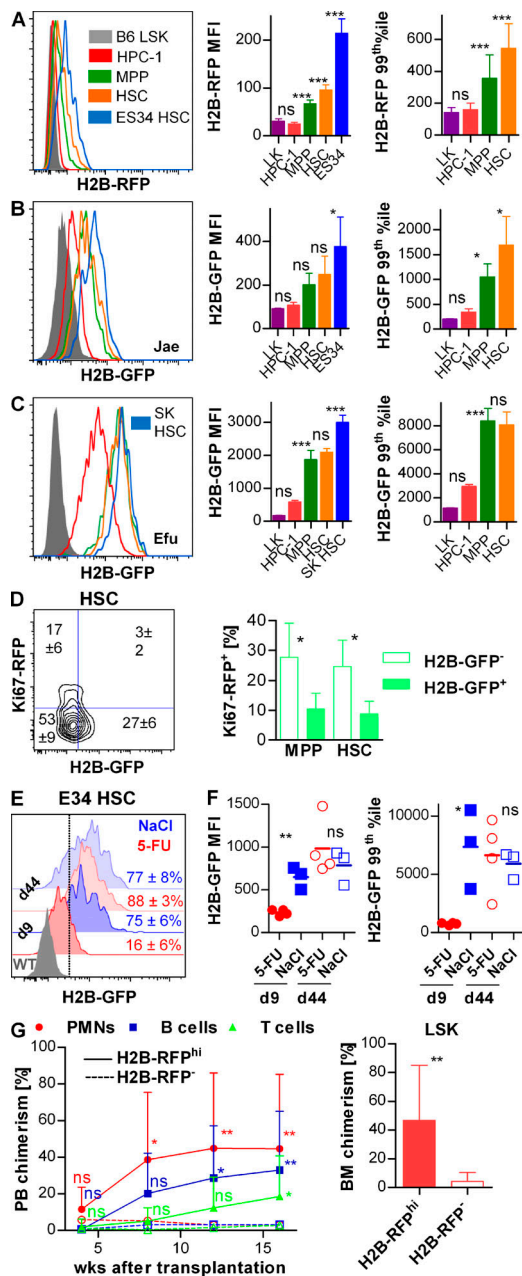


**Figure 1. Primitive HSPCs exhibit higher levels of leaky H2B-FP background fluorescence. (A–C)** BM HSPCs from repressed H2B-FP transgenic mouse models were analyzed for background fluorescence by flow cytometry. Histograms (left panels) show representative examples of H2B-FP background fluorescence of HSPC populations (LSK:  $lin^{-/lo}Sca-1^{hi}Kit^{+}$ ; HPC-1: LSK  $CD48^{hi}CD150^{-}$  [red]; MPP: LSK  $CD48^{-/lo}CD150^{-}$  [green]; HSC: LSK  $CD48^{-/lo}CD150^{+}$  [orange]; ES34 HSC:  $lin^{-/lo}Sca-1^{hi}Kit^{+} CD48^{-/lo}CD150^{+} CD201^{hi}CD34^{-/lo}$  [blue, A and B]; SK HSC:  $lin^{-/lo}Sca-1^{hi}Kit^{lo} CD48^{-/lo}CD150^{+}$  [blue, C]; LK:  $lin^{-/lo}Sca-1^{hi}Kit^{+}$  [purple]; see Fig. S1 A for detailed gating strategy). LSK cells from WT B6 mice served as autofluorescence controls (gray tinted histogram). Median fluorescence intensity (MFI, middle data plot) and maximum (99th percentile, right data plot) fluorescence intensity of BM HSPCs were determined. Significance was calculated by one-way repeated-measures ANOVA with Bonferroni correction for multiple testing. **(A)** H2B-RFP background fluorescence of HSPCs isolated from un-induced  $R26^{rtTA}/Col1A1^{H2B-RFP}$  mice ( $n = 12$ , 10–17 wk of age, pooled from three independent experiments),  $Col1A1^{H2B-RFP}/H2B-RFP$  ( $n = 3$ ) and  $Col1A1^{H2B-RFP}/wt$  ( $n = 9$ ), zygosity was corrected by doubling the fluorescence of heterozygous mice; see

division-independent degradation of H2B-GFP and H2B-RFP to proceed in HSCs with half-lives of ~4–6 and 2 wk, respectively, and show that neglect of H2B-FP decay leads to overestimation of HSC mitotic activity. Two sequential rounds of H2B-RFP induction and subsequent dilution revealed that HSCs do not abruptly halt mitotic activity upon aging, arguing against sudden entry of HSCs into permanent quiescence after four divisions as previously hypothesized (Bernitz et al., 2016). Mathematical modeling of H2B-FP systems revealed that background label accumulates over time in the most primitive and quiescent HSCs, providing an explanation for observing seemingly stable label-retaining HSCs after extended chase periods. We argue that such cells were previously misinterpreted as permanently quiescent HSCs.

## Results

### Primitive hematopoietic stem and progenitor cells (HSPCs) exhibit higher levels of leaky H2B-FP background fluorescence

Upon flow-cytometric analysis of HSPC populations (Fig. S1 A) isolated from bone marrow (BM) of deliberately un-induced  $R26^{rtTA}/Col1A1^{H2B-RFP}$  (Egli et al., 2007),  $R26^{rtTA}/Col1A1^{H2B-RFP}$  (Foudi et al., 2009), or single transgenic tetO-H2B-GFP47Efu (Bernitz et al., 2016; Tumber et al., 2004) mice, we observed a gradual increase of median and maximum (as judged by the 99th percentile) background H2B-FP fluorescence from fast cycling

Fig. S1 B. **(B)** H2B-GFP background fluorescence of HSPCs isolated from un-induced  $R26^{rtTA}/rtTA/Col1A1^{H2B-GFP}/H2B-GFP$  (Jae) mice ( $n = 4$ , 22 wk of age, representative of five independent experiments). **(C)** H2B-GFP background fluorescence of HSPCs isolated from single transgenic tetO-H2B-GFP47Efu/J animals ( $n = 3$ , homozygous, 10 wk of age). **(D)** HSPCs from un-induced  $Ki67^{RFP}/wt/R26^{rtTA}/wt/Col1A1^{H2B-GFP}/wt$  mice ( $n = 6$ , age 12–15 wk) were analyzed for Ki67-RFP and H2B-GFP expression (left, representative contour plot of the HSC population, mean frequency  $\pm$  SD of each quadrant is shown). Thresholds for Ki67-RFP and H2B-GFP gating were set according to either  $Ki67^{RFP}/wt$  or  $R26^{rtTA}/wt/Col1A1^{H2B-GFP}/wt$  single-positive animals (not shown). The frequency of proliferative Ki67-RFP<sup>+</sup> cells within H2B-GFP<sup>-</sup> or H2B-GFP<sup>+</sup> MPPs and HSCs was calculated (right data plot, significance was analyzed by Wilcoxon's signed-rank test). **(E and F)** Repressed  $R26^{rtTA}/rtTA/Col1A1^{H2B-GFP}/H2B-GFP$  mice (11–16 wk of age) were injected with 5-FU (shown in red,  $n = 8$ ) or 0.9% saline (blue,  $n = 6$ ), and BM was analyzed 9 or 44 d later by flow cytometry. **(E)** Representative histograms of H2B-GFP fluorescence in  $CD201^{hi}CD34^{-/lo}$  LSK  $CD48^{-/lo}CD150^{+}$  cells (E34 HSCs) are shown. H2B-GFP<sup>+</sup> cells (mean frequency  $\pm$  SD shown) were gated according to a 5-FU-treated WT mouse (autofluorescence control, gray histogram). **(F)** H2B-GFP median (left) and maximum (99th percentile, right) fluorescence intensity of E34 HSCs from 5-FU and saline-treated  $R26^{rtTA}/rtTA/Col1A1^{H2B-GFP}/H2B-GFP$  individual mice are shown (significance was calculated by un-paired Student's *t* test). **(G)** 50 H2B-RFP<sup>-</sup> or H2B-RFP<sup>hi</sup> HSCs were purified from un-induced  $R26^{rtTA}/wt/Col1A1^{H2B-RFP}/wt$  animals ( $n = 4$ , 9–12 wk; see Fig. S2 G for sorting strategy) and transplanted together with  $3 \times 10^5$  B6.CD45.1 WBMCs into irradiated B6.CD45.1/2 recipient mice ( $n = 8$  or 9 per group). PB (left plot) neutrophils (PMN,  $CD11b^{+}Gr-1^{hi}$ ), B- ( $CD19^{+}$ ) and T-lymphocytes ( $CD3^{+}$ ) of chimeric recipients were analyzed for donor origin at indicated time points (mean and SD are shown, significance was calculated by repeated measures two-way ANOVA with Bonferroni post-test). BM LSK chimerism was determined 17 wk after transplantation (right plot, un-paired Student's *t* test). An independent replicate of this experiment including secondary transplantation is shown in Fig. S2 H. \*,  $P = 0.01$ –0.05; \*\*,  $P = 0.001$ –0.01; \*\*\*,  $P < 0.001$ ; ns, not significant.

hematopoietic progenitor cells (HPCs) to quiescent HSCs (Fig. 1, A–C). Interestingly, within the immuno-phenotypic HSC population (LSK CD48<sup>-lo</sup>CD150<sup>+</sup>), we found particularly bright H2B-FP background fluorescence in the predominantly quiescent CD201<sup>hi</sup>Sca-1<sup>hi</sup>CD34<sup>-lo</sup> (E34) HSC subpopulation. Among HSCs with high background fluorescence from all three different repressed H2B-FP mouse strains under investigation, we observed significantly higher expression of Sca-1, CD201, and CD150 as well as concordant down-regulation of CD34, CD48, and CD117 (Fig. S1, C–E) compared with cells without H2B-FP background fluorescence. This expression pattern of surface markers has been previously correlated to increased quiescence and repopulation activity of HSCs (Beerman et al., 2010; Grinenko et al., 2014; Kent et al., 2009; Kiel et al., 2005; Morcos et al., 2017; Osawa et al., 1996; Sato et al., 1999; Säwén et al., 2016; Shin et al., 2014; Wilson et al., 2015). To further investigate the cell cycle status of HSPCs in relation to H2B-GFP background fluorescence, we analyzed the BM of un-induced Ki67<sup>RFP/wt</sup>/R26<sup>rtTA/wt</sup>/Col1A1<sup>H2B-GFP/wt</sup> mice, in which Ki67-RFP expression reports cycling cells (Basak et al., 2014; Morcos et al., 2017). We observed a significantly lower fraction of cycling Ki67-RFP<sup>+</sup> cells among HSCs and multipotent progenitors (MPPs) with high H2B-GFP background (Fig. 1 D). In addition, we performed transcriptome analysis of 200 single HSCs, which were indexed from un-induced R26<sup>rtTA/rtTA</sup>/Col1A1<sup>H2B-GFP/H2B-GFP</sup> animals, and found a quiescence-related gene signature up-regulated in HSCs with high H2B-GFP background fluorescence (Fig. S2, A–E).

To prove that H2B-FP background fluorescence depends on recent mitotic activity, we injected un-induced R26<sup>rtTA/rtTA</sup>/Col1A1<sup>H2B-GFP/H2B-GFP</sup> mice with 5-fluorouracil (5-FU), which has been shown to force quiescent HSCs into cell cycle (Harrison and Lerner, 1991; Wilson et al., 2008). Peripheral blood (PB) analysis 6 d later revealed uniform myelo-ablation in 5-FU-treated animals (Fig. S2 F). The H2B-GFP background fluorescence of BM CD201<sup>hi</sup>CD34<sup>-lo</sup> (E34) HSCs isolated from 5-FU injected mice 9 d after treatment was strongly reduced compared with saline-injected control mice (Fig. 1, E and F). A sub-cohort of animals was analyzed 44 d after 5-FU treatment and revealed that E34 HSCs had reestablished high background fluorescence, similar to saline-treated control mice. This clearly demonstrated that enforced mitotic activity of HSCs led to temporary, cell cycle-dependent reduction of H2B background fluorescence.

As predominantly quiescent HSCs with a primitive immuno-phenotype exhibited bright H2B-FP background fluorescence, we reasoned that high background might identify HSCs with superior repopulating activity upon transplantation. Therefore, HSCs from un-induced R26<sup>rtTA/wt</sup>/Col1A1<sup>H2B-RFP/wt</sup> donor mice were separated into H2B-RFP<sup>-</sup> and H2B-RFP<sup>hi</sup> populations (Fig. S2 G) and transplanted along with WT whole BM competitor cells into lethally irradiated congenic recipient mice. PB and BM analysis of primary and secondary recipient mice (Fig. 1 G and Fig. S2 H) revealed that H2B-RFP<sup>-</sup> donor HSCs contained little long-term repopulation activity, while transplantation of H2B-RFP<sup>hi</sup> donor HSCs resulted in robust serial multi-lineage repopulation. Taken together, our experiments demonstrated that primitive HSCs accumulated high H2B-FP background fluorescence, while HSCs with dull background divided more

frequently, up-regulated transcription- and translation-related genes, and had significantly lower repopulation potential. Since all HSPC populations exhibited considerable background fluorescence and reacquired background after temporary reduction in response to 5-FU, we conclude that there is continuous leaky background expression of H2B-FP even in the absence of label induction.

### Major contribution of H2B-FP degradation to loss of label

We observed much faster dilution of H2B-RFP (Morcos et al., 2017; Säwén et al., 2016) compared with H2B-GFP (Foudi et al., 2009; Oguro et al., 2013) in label retention experiments (Fig. 2 A) using homologous Tet-controlled R26<sup>rtTA</sup>/Col1A1<sup>H2B-FP</sup> transgenic systems (Beard et al., 2006) and suspected this to be caused by different stability of both H2B-FPs. To determine the rate of H2B-FP degradation, we assumed that, within short chase intervals, at least a fraction of HSCs displaying the highest H2B-FP retention will remain quiescent and will not or very rarely divide within this time period. Thus, over short chase intervals, the loss of fluorescence in those HSCs expressing the brightest H2B-FP fluorescence at each time point of analysis can be attributed to H2B-FP degradation. A similar approach in epithelial stem cells previously determined an H2B-GFP protein half-life of 24 d (Waghmare et al., 2008). Accordingly, we plotted a fluorescence time course of HSCs (Fig. 2 B) and MPPs (Fig. S2 I) with maximum label retention isolated from pulsed and chased R26<sup>rtTA</sup>/Col1A1<sup>H2B-RFP</sup> and R26<sup>rtTA</sup>/Col1A1<sup>H2B-GFP</sup> mice and estimated absolute protein degradation half-lives of around 2 and 6 wk for H2B-RFP and H2B-GFP, respectively. To unambiguously prove the different stability of both H2B-FPs, we generated R26<sup>rtTA</sup>/Col1A1<sup>H2B-GFP/H2B-RFP</sup> mice in which both labels are simultaneously expressed. A pulse-chase experiment using these mice revealed much faster decay of H2B-RFP than H2B-GFP and verified previously estimated protein half-lives (Fig. 2, C–E). These rather short half-lives demonstrate that protein degradation is the major process responsible for loss of H2B-FP in quiescent HSCs. Therefore, neglecting this process must result in massive overestimation of HSC divisional activity.

As a gedankenexperiment, we neglect division-independent label degradation as implied by Bernitz et al. (2016) and further adhere to their conclusion that primitive HSCs undergo only four symmetric self-renewal divisions within the first 9 mo of their lives before they completely stop dividing. Under these assumptions, the H2B-FP dilution kinetics of young (<9 mo) and aged (>9 mo) mice should strongly differ from each other. To contest this prediction, we performed two consecutive cycles of doxycycline (DOX) induction and successive chase of R26<sup>rtTA</sup>/Col1A1<sup>H2B-RFP</sup> mice (Fig. 2 F). We found similar labeling of HSCs after the first and second round of pulse. Cohorts of mice were analyzed after the first and second chase cycle, and we observed highly similar label dilution in young and aged HSCs. If both label degradation had been absent and HSCs had entered permanent quiescence upon aging, we would have observed a subpopulation of HSCs retaining high levels of label after the second pulse. Competitive transplantation after the second pulse-chase cycle revealed an enrichment of repopulation activity among H2B-RFP<sup>+</sup> cells, but also the H2B-RFP<sup>-</sup> fraction

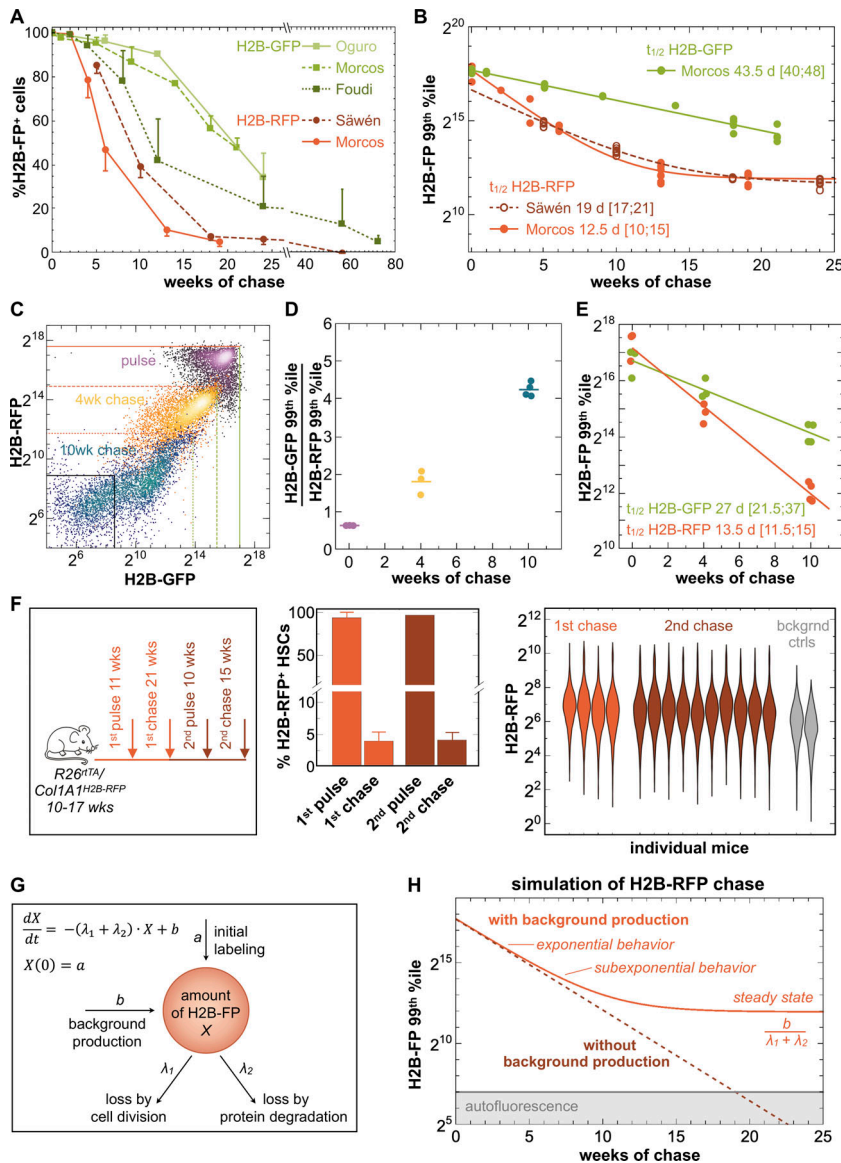


**Figure 2. Major contribution of H2B-FP degradation to loss of label.** (A) The frequencies of label-retaining (H2B-FP<sup>+</sup>) HSCs from pulsed and chased *R26<sup>rtTA</sup>/Col1A1<sup>H2B-FP</sup>* mice are shown (H2B-RFP, red; H2B-GFP, green). Data were retrieved from Foudi et al. (2009), Oguro et al. (2013), Säwén et al. (2016), and Morcos et al. (2017). H2B-GFP Morcos: *R26<sup>rtTA/rtTA</sup>/Col1A1<sup>H2B-GFP/H2B-GFP</sup>* mice ( $n = 1-4$ /time point, pooled from two independent experiments) were fed for 3 wk with DOX chow (2 g/kg) and chased for 0–21 wk. Mean frequencies and SD of LSK CD48<sup>-/lo</sup>CD150<sup>+</sup> cells are shown, except for data from Oguro et al. (2013), in which a weighted mean of the HSC-1 and HSC-2 subpopulations was calculated ( $[1 \times \text{HSC-1} + 3 \times \text{HSC-2}]/4$ ). (B) Maximum H2B-FP fluorescence intensities (as judged by the 99th percentile) of HSCs (LSK CD48<sup>-/lo</sup>CD150<sup>+</sup>) isolated from chased *R26<sup>rtTA</sup>/Col1A1<sup>H2B-RFP</sup>* (shown in red; Säwén et al., 2016, dashed line, open circles; Morcos et al., 2017, continuous line, filled circles) or *R26<sup>rtTA/rtTA</sup>/Col1A1<sup>H2B-GFP/H2B-GFP</sup>* (green; same animals as in A “GFP Morcos”) individual mice are depicted. The data were fitted by our mathematical model (see G), and loss of maximum fluorescence was attributed to H2B-FP degradation. H2B-FP half-lives and respective 95% confidence intervals (squared brackets) were calculated. (C–E) LSK CD48<sup>-/lo</sup>CD150<sup>+</sup> HSCs of either pulsed (2 g DOX/kg chow ad libitum for 7 wk; shown in purple), 4 (yellow), or 10 (blue) wk-chased *R26<sup>rtTA/wt</sup>/Col1A1<sup>H2B-GFP/H2B-RFP</sup>* mice ( $n = 3$  or  $4$ /each time point) were analyzed for H2B-GFP and H2B-RFP fluorescence. (C) Representative examples of HSCs from either pulsed, 4 or 10 wk-chased *R26<sup>rtTA/wt</sup>/Col1A1<sup>H2B-GFP/H2B-RFP</sup>* animals. Lines depict maximum (99th percentile) H2B-GFP (shown in green) and H2B-RFP (red) fluorescence intensities of pulsed (continuous lines) and chased (dotted lines) mice. Black lines depict the maximum background fluorescence intensities from un-induced *R26<sup>rtTA/wt</sup>/Col1A1<sup>H2B-GFP/H2B-RFP</sup>* controls. (D) The ratio of maximum H2B-GFP and H2B-RFP fluorescence intensity in HSCs was calculated for pulsed and chased animals (individuals and means are shown). (E) Time course of maximum H2B-GFP and H2B-RFP fluorescence of HSCs isolated from pulsed and chased *R26<sup>rtTA/wt</sup>/Col1A1<sup>H2B-GFP/H2B-RFP</sup>* individuals. Calculation of H2B-FP half-lives and respective 95% confidence intervals (squared brackets) was performed as in B. (F) *R26<sup>rtTA/wt</sup>/Col1A1<sup>H2B-RFP/wt</sup>* mice ( $n = 21$ , 10–17 wk of age) were

subjected to two consecutive cycles of H2B-RFP labeling by DOX induction (625 mg DOX/kg chow ad libitum for 10–11 wk, “pulse”) and dilution (“chase”). Cohorts of animals were sacrificed at indicated time points for BM analysis (LSK CD48<sup>-/lo</sup>CD150<sup>+</sup>). Frequencies of H2B-RFP<sup>+</sup> HSCs (middle panel, LSK CD48<sup>-/lo</sup>CD150<sup>+</sup>) were analyzed after the first ( $n = 4$  animals) and second ( $n = 10$ ) pulse-chase cycle. Violin plots (right panel) depict H2B-RFP fluorescence distributions of individual mice after the first and second chase cycle. Un-induced *R26<sup>rtTA/wt</sup>/Col1A1<sup>H2B-RFP/wt</sup>* mice (gray, 12 wk of age) served as background controls. (G) Overview of the ordinary differential equation model describing label dilution by accounting for four processes that affect average H2B-FP labeling intensity ( $X$ ): (i) initial labeling  $a$  by H2B-FP induction, (ii) permanent leaky background H2B-FP production with constant rate  $b$ , (iii) H2B-FP decay due to division with rate  $\lambda_1$ , and (iv) division-independent decay due to H2B-FP protein degradation with rate  $\lambda_2$  (for details see Materials and methods). (H) Simulation of H2B-RFP label decay over time in pulsed and chased mice in the absence (dark red, dashed) or presence (red, continuous line) of continuous leaky background production. Gray area reflects autofluorescence.

contained HSCs with long-term, multi-lineage potential (Fig. S2 J). Taken together, this experiment strongly argues against abrupt entry into permanent quiescence in the absence of label degradation in aging HSCs.

**Mathematical modeling to quantify label dilution kinetics**

To quantify the impact of leaky background expression and division-independent degradation of H2B-FPs, we complemented the findings described above by a simple mathematical modeling approach accounting for key features of a

pulse-chase experiment (Fig. 2 G). In particular, the model describes the kinetics of the average H2B-FP intensity  $X$  that is subject to four processes: (i) initial labeling  $a$  in case of H2B-FP induction, (ii) permanent leaky background H2B-FP production with constant rate  $b$ , (iii) H2B-FP decay due to division with rate  $\lambda_1$ , and (iv) division-independent decay due to H2B-FP protein degradation with rate  $\lambda_2$ .

In the absence of leaky background production, the model reduces to an exponential decay process, which does not reproduce the observed background expression above

autofluorescence levels (Fig. 2 H). In contrast, assuming constant background label production, the model follows the pattern observed in pulse-chase experiments: during the initial chase period, the curves with or without additional leaky background production display the same exponential loss of label. However, after longer chase periods, when label intensities reach the range of background fluorescence, the effect of continuous background production becomes prominent and leads to sub-exponential label loss by gradual slowing down until reaching a constant background level. This final background level is characterized by a balance between the leaky background production rate  $b$  and the sum of the two decay processes  $\lambda_1$  and  $\lambda_2$ , but does not depend on the initial amount of label. This explains the observation of higher H2B-FP background fluorescence in populations with less proliferative activity: a lower division rate  $\lambda_1$  results in a higher final H2B-FP accumulation.

In summary, the mathematical modeling strongly suggests that continuous leaky background expression is critical to explain the observed nonexponential dynamics of label dilution. We show that the final level of background fluorescence depends on both the degradation half-life of the FP and the mitotic activity of the cell population under investigation, but not on the initial amount of label in pulse-chase experiments.

#### Age-dependent accumulation of H2B-FP background fluorescence

Based on our observation that quiescent HSPCs isolated from repressed H2B-FP mice exhibit high background fluorescence, we propose a scenario in which HSPC subpopulations start to accumulate H2B-FP background fluorescence upon entering extended phases of quiescence in early postnatal life (Bowie et al., 2006), while more proliferative cells will continue to constantly dilute background label via mitosis. In fact, mathematical modeling predicted that the accumulation of maximum H2B-FP background fluorescence would take weeks to several months after cessation of rapid cell divisions in early postnatal development (Fig. 3 A). The length of this time span depends on stability of H2B-FP as well as mitotic activity of the cell population under investigation. In case of the more stable H2B-GFP, our simulation predicted a time span of up to 1 yr for full background accumulation. To rigorously test these predictions, we analyzed repressed mice of different ages from three H2B-FP transgenic mouse strains and found an age-dependent increase of median and maximum background fluorescence in various HSPC populations (Fig. 3, B–D). Our analysis revealed that (i) more quiescent HSPC populations took longer to build up final background fluorescence levels (e.g., HPC-1 < MPP < HSC) and (ii) the median and maximum background of HSPCs from all H2B-FP mouse models under investigation approached a plateau in older animals. These findings strongly confirmed the predictions derived from our mathematical model. A control analysis of differently aged WT B6 mice excluded any potential age-dependent increase of autofluorescence (Fig. 3, B–D).

In summary, our data clearly demonstrate that H2B-FP background fluorescence of primitive HSCs progressively accumulated with age. Therefore, age-matched littermate

background controls are crucial for accurate identification of H2B-FP-retaining HSCs in pulse-chase experiments.

#### Mitotic activity of HSC populations inferred from H2B-FP label dilution data

We evaluated HSC label retention data by our mathematical model in order to disentangle the different sub-processes which account for loss of label (i.e., protein degradation, leaky background production, and cell division). To resolve and quantify mitotic heterogeneity, we fitted different Gaussian distributions to the H2B-FP histograms of chased HSCs (Fig. 4 A and Fig. S3, A and B). For H2B-RFP-labeled HSCs, we identified two peaks (RFP<sup>lo</sup> and RFP<sup>hi</sup>) throughout the entire chase (2–19 wk), while for chased HSCs expressing H2B-GFP, we initially found two peaks (GFP<sup>lo</sup> and GFP<sup>hi</sup>), but starting from 14 wk of chase, a third, intermediate population (GFP<sup>mid</sup>) appeared in all replicates (Fig. 4, A and B).

For the most proliferative HSC subset, i.e., the cells that displayed the fastest loss of fluorescence (RFP<sup>lo</sup> and GFP<sup>lo</sup>), we estimated an identical mean division rate of once per ~23 d from both H2B-RFP and H2B-GFP label dilution datasets (Fig. 4 C). This consistent division rate proved that the threefold difference in protein stability of H2B-GFP compared with H2B-RFP ( $t_{1/2}$  ~6 and 2 wk, respectively) accounted for their fundamentally different label retention characteristics (Fig. 2 A), while the genuine cell cycle activity of this HSC subset was not altered by the H2B-FP itself. Next, we analyzed H2B-FP dilution of predominantly quiescent HSC subpopulations, which retained higher levels of label. For the RFP<sup>hi</sup> HSC population, we determined an average division rate of ~1/159 d. Using our H2B-GFP dataset, we estimated no or very rare divisions for the few GFP<sup>hi</sup> HSCs, while the GFP<sup>mid</sup> population, which appeared after 4 mo of chase, displayed an average proliferation rate of 1/56 d. However, since protein degradation was the main reason for loss of label in quiescent HSCs, even in case of the more stable H2B-GFP, we found that our estimated division rates of predominantly quiescent RFP<sup>hi</sup> and GFP<sup>hi</sup> HSCs were highly imprecise, as evidenced by their broad confidence intervals and a pronounced impact of the estimated H2B-FP protein degradation rate on the predicted division rate (Fig. 4 D). We conclude that the immunophenotypic HSC population displays heterogeneous cell cycle activity and that the most quiescent HSCs of adult mice cycle infrequently (<1/100 d) and some may possibly never divide during the animal's adulthood. However, our analysis of label retention data did not provide evidence for a subpopulation of HSCs undergoing a traceable number of self-renewal divisions before suddenly entering permanent quiescence.

#### Discussion

Our results demonstrate that loss of label in HSCs using different H2B-FPs is not only determined by label dilution via mitosis, but is additionally governed by division-independent degradation as well as leaky background production of label. We show that repressed H2B-FP mouse models including the single transgenic B6.tetO-H2B-GFP47Efu background controls employed by Bernitz et al. (2016) progressively accumulate background

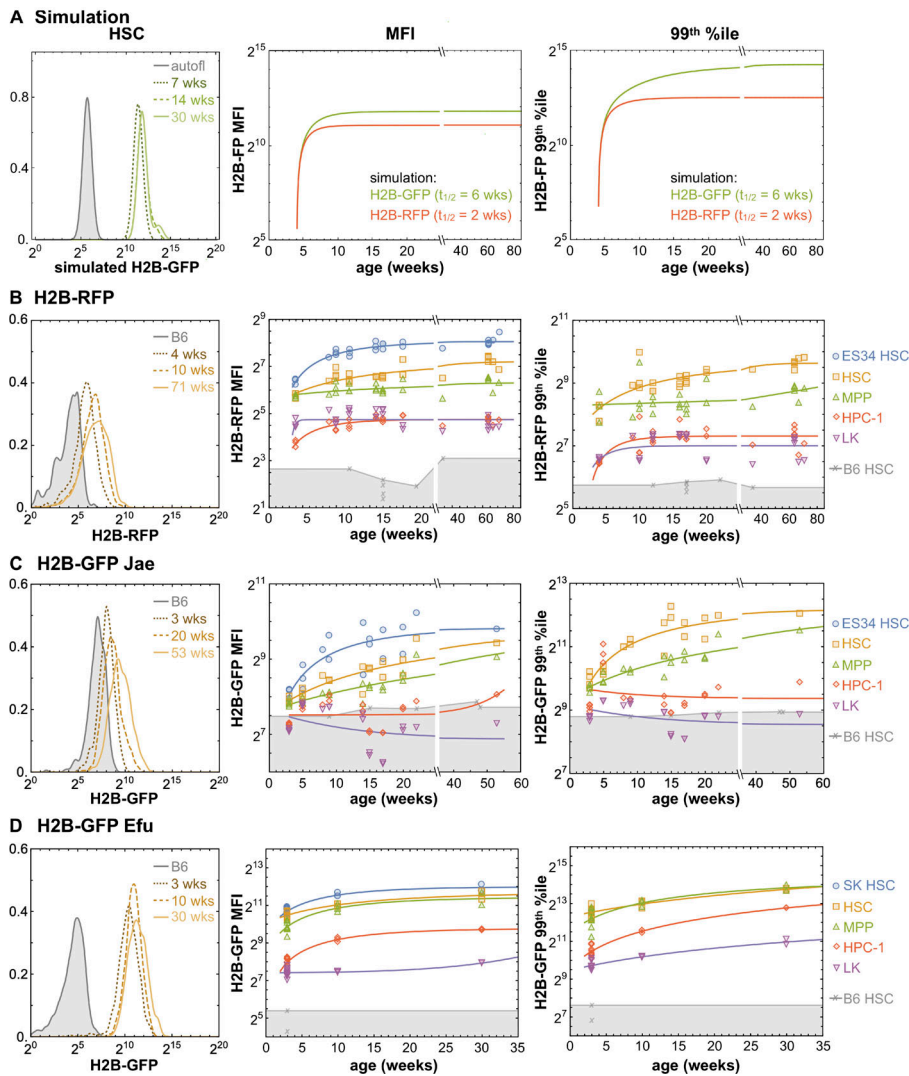


**Figure 3. Age-dependent accumulation of H2B-FP background fluorescence.** (A) Simulation of background labeling in repressed H2B-FP mouse models revealed accumulation of background fluorescence in predominantly quiescent HSCs upon aging. Simulated H2B-GFP fluorescence distributions (left histograms) of HSCs from differently aged background controls are depicted. Median (MFI, middle panel) and maximum (99th percentile, right panel) fluorescence intensities of HSCs expressing either H2B-GFP (shown in green, degradation  $t_{1/2} = 6$  wk) or H2B-RFP (red, degradation  $t_{1/2} = 2$  wk) background were simulated under the assumption that adult hematopoiesis is established after 4 wk of age (see also Materials and methods). (B–D) BM HSPCs isolated from repressed H2B-FP mouse strains of various ages were analyzed for H2B-FP background fluorescence by flow cytometry. Representative examples of BM HSCs (LSK CD48<sup>-lo</sup>CD150<sup>+</sup>) depict the age-dependent increase of H2B-FP background fluorescence (left histograms). Median (MFI, middle data plots) and maximum (99th percentile, right data plots) H2B-FP fluorescence intensity of BM HSPCs were determined. Individual mice are shown; curves show fits of the mathematical model. HSCs from WT B6 mice (3–48 wk of age, gray crosses) served as autofluorescence controls. (B) H2B-RFP background fluorescence of HSPCs isolated from un-induced *R26<sup>rtTA</sup>/Col1A1<sup>H2B-RFP</sup>* mice ( $n = 25$ , pooled from five independent experiments), *Col1A1<sup>H2B-RFP/H2B-RFP</sup>* ( $n = 11$ ) and *Col1A1<sup>H2B-RFP/wt</sup>* ( $n = 14$ , zygosity was corrected by doubling the fluorescence of heterozygous mice). (C) H2B-GFP background fluorescence of HSPCs isolated from un-induced *R26<sup>rtTA/rtTA</sup>/Col1A1<sup>H2B-GFP/H2B-GFP</sup>* mice ( $n = 20$ , pooled from four independent experiments). (D) H2B-GFP background fluorescence of HSPCs isolated from single transgenic tetO-H2B-GFP47Efu/ animals ( $n = 13$ , homozygous:  $n = 5$ , hemizygous:  $n = 8$ , zygosity was corrected by doubling the fluorescence of hemizygous mice).

fluorescence upon aging to finally reach an equilibrium state in which loss of label and leaky background production are balanced. Consequently, high background fluorescence per se enriches for the most quiescent HSCs with a CD201<sup>hi</sup>, Sca-1<sup>hi</sup> and CD34<sup>-lo</sup> immuno-phenotype and enhanced repopulation potential. We identified division-independent H2B-FP protein degradation as the major reason for loss of pulsed label in HSCs, precluding extended chase experiments and exact determination of mitotic history of quiescent HSCs. Nonetheless, our analysis of H2B-FP dilution data revealed infrequent but steady mitosis of primitive adult HSCs.

#### No evidence for abrupt entry of HSCs into permanent quiescence after four discrete divisions

Bernitz et al. (2016) proposed that a population of murine HSCs enters permanent quiescence after four symmetric self-renewal divisions within the first year of life. The authors hypothesized that these cells must count and remember their mitotic history

by a yet unknown mechanism. This hypothesis is entirely based on the observation of a small HSC population with high repopulation potential seemingly retaining pulsed H2B-GFP fluorescence above background for up to 22 mo of chase. While we disagree with their interpretation, the experimental results by Bernitz et al. (2016) are in good agreement with previous (Foudi et al., 2009; Qiu et al., 2014; Wilson et al., 2008) as well as our own findings. Most prominently, Bernitz et al. (2016) consistently report a superior repopulation activity and increased quiescence of the HSC subpopulation with the highest levels of H2B-GFP fluorescence after long-term chase. However, their analysis does not account for continuous de novo H2B-GFP background production and its age-dependent and inevitable accumulation in quiescent HSC with high repopulation potential. Our data strongly suggest that quiescent HSCs with high background accumulation were mistaken for HSCs permanently retaining pulsed label, presumably by the use of inappropriate background controls (Fig. S4 A). The unambiguous

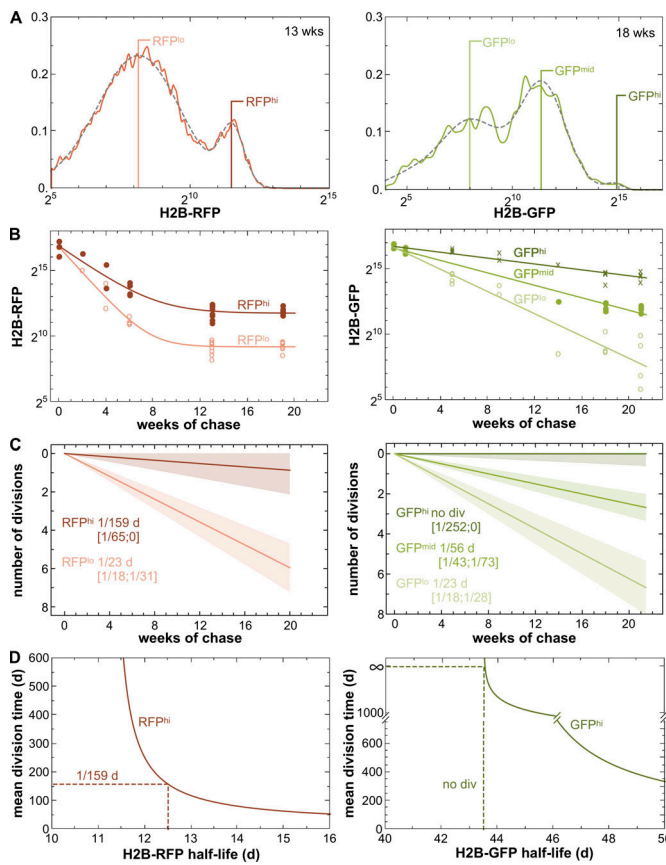


**Figure 4. Mitotic activity of HSC populations inferred from H2B-FP label dilution data.** (A) Representative examples for mixtures of Gaussian distributions fitted to H2B-RFP (left panel,  $R26^{rtTA}/Col1A1^{H2B-RFP}$  animals;  $n = 1-9$ /time point, pooled from three independent experiments, data from Morcos et al., 2017) or H2B-GFP (right panel,  $R26^{rtTA/rtTA}/Col1A1^{H2B-GFP/H2B-GFP}$  mice shown in Fig. 2, A and B) label dilution data of HSCs (continuous curves: recorded data; dotted gray curves: fitted mixture distributions). Two Gaussians ( $RFP^{lo}$  and  $RFP^{hi}$ , light and dark red, respectively) were fitted to H2B-RFP retention data (0–19 wk of chase), while for H2B-GFP retention data (0–21 wk of chase) two peaks ( $GFP^{lo}$  and  $GFP^{hi}$ ) were initially observed, but starting from 14 wk, a third, intermediate peak uniformly appeared ( $GFP^{mid}$ ). The mean (horizontal lines) of each fitted Gaussian was estimated (see also Fig. S3, A and B). (B) H2B-FP dilution time courses of Gaussian distributions fitted to H2B-RFP (left;  $RFP^{lo}$ : light red, open circles;  $RFP^{hi}$ : dark red, filled circles) and H2B-GFP (right panel;  $GFP^{lo}$ : light green, open circles;  $GFP^{mid}$ : intermediate green, filled circles;  $GFP^{hi}$ : dark green, crosses) HSC (LSK CD48<sup>-/lo</sup>CD150<sup>+</sup>) label retention data were plotted (curves show fits of the mathematical model; symbols depict means of fitted Gaussians from individual mice). (C) Division rates and their respective 95% confidence intervals (tinted areas and squared brackets) of  $RFP^{lo}$  and  $RFP^{hi}$  (left panel, red) or  $GFP^{lo}$ ,  $GFP^{mid}$ , and  $GFP^{hi}$  (right panel, green) HSCs were calculated from data shown in B (for analysis of the CD34<sup>-/lo</sup> HSC population, see Fig. S3 C). (D) Model plots illustrating the dependence of the inferred mean division time within the most quiescent  $RFP^{hi}$  (left) or  $GFP^{hi}$  (right) HSC population on the accuracy of estimated H2B-FP degradation half-lives. Dotted lines depict the derived division rates for  $RFP^{hi}$  and  $GFP^{hi}$  HSCs based on the estimated H2B-RFP and H2B-GFP half-lives of 12.5 and 43.5 d, respectively.

identification of cells with minute levels of H2B-GFP retention, as reported by Bernitz et al. (2016), is further complicated by the considerable inter-individual variation of H2B-FP maximum background fluorescence within control mice of the same age (Fig. 3, B–D).

Another serious concern regarding the validity of prolonged H2B-FP pulse-chase experiments is division-independent label degradation. For H2B-GFP, we determined a protein half-life of ~4–6 wk in HSCs, which is similar to its stability in epithelial stem cells (Waghmare et al., 2008). Consequently, protein degradation on its own will reduce H2B-GFP fluorescence at least 500-fold, i.e., to undetectable levels, already after 1 yr of chase (or  $>10^5$ -fold after 22 mo of chase; Fig. S4 B). This applies to all H2B-GFP transgenes that share the same amino acid sequence. Our finding of substantial division-independent H2B-FP degradation is in line with the fact that various DNA transactions, e.g., transcription, require histone displacement from DNA (Venkatesh and Workman, 2015). Even in nonreplicating cells, high protein turnover was shown for endogenous H2B as well as for H2B-GFP (Jamai et al., 2007; Kimura and Cook, 2001; Toyama et al., 2013). Our pulse-chase experiment using mice with simultaneous expression of both H2B-FPs confirmed that the two fusion proteins differ in their stability. Moreover, two successive rounds of H2B-FP pulse-chase revealed unaltered label dilution in young and old mice (Fig. 2 F). This finding is not compatible with abrupt entry of aging HSCs into permanent quiescence together with absence of H2B-FP degradation.

Finally, we rebut counting of discrete HSC divisions using H2B-FP mouse models due to their inhomogeneous initial labeling. Bernitz et al. (2016) report an initial labeling distribution of  $\sim 2 \log_{10}$  of H2B-GFP fluorescence as well as a considerable fraction of un-labeled HSCs (i.e., below background fluorescence; Qiu et al., 2014). This might be explained by variable, HSC subset-specific activity of the human CD34 (Radomska et al., 2002) promoter driving H2B-GFP labeling in this model. Use of the ubiquitous  $R26^{rtTA}$  Tet-driver with either  $Col1A1^{H2B-FP}$  allele resulted in a more homogenous initial H2B-FP distribution of pulsed HSCs with virtually 100% labeling above background and a peak width of  $\sim 1 \log_{10}$  (Foudi et al., 2009; Li et al., 2013; Nakada et al., 2014; Säwén et al., 2016; Fig. S4 C). However, the broad initial HSC labeling range of  $\sim 1-2 \log_{10}$  of fluorescence intensity translates into three to six division equivalents already at start of chase. This broad heterogeneity renders counting of discrete HSC divisions impossible, which is in contrast to successful tracing of discrete divisions in homogeneously pulsed epithelial stem cells (Waghmare et al., 2008). A more homogeneous labeling of a primitive HSC subpopulation that might be hidden within immuno-phenotypic HSCs was not detected (Fig. S4, D and E). Our modeling of H2B-FP retention revealed that loss of label slows down when cells approach the range of background fluorescence due to continuous de novo background production (Fig. 2, B and H; and Fig. S4 A). Therefore, mitosis of cells retaining pulsed label in the range of background fluorescence does not lead to halving of H2B-FP fluorescence and further obscures resolution of discrete division events within these cells.

While we found no evidence for HSCs counting and remembering discrete cell divisions from H2B-FP label retention experiments, we appreciate that HSCs were shown to gradually lose stem cell potential with increasing numbers of divisions, and thus quiescence and self-renewal potential of HSCs are tightly linked (Fleming et al., 1993; Foudi et al., 2009; Passegué

et al., 2005; Qiu et al., 2014; Spangrude and Johnson, 1990; Wilson et al., 2008). Our data confirm this longstanding notion. However, we do not find evidence for sudden and complete loss of self-renewal potential upon a fifth HSC division.

### HSC mitotic activity in unperturbed adult BM inferred from H2B-FP dilution

The rather short protein half-lives of H2B-FPs complicate the accurate estimation of mitotic activity in pulse-chase experiments as the major loss of label in primitive HSCs, which are predominantly quiescent, results from degradation rather than proliferation. Therefore, complete disentanglement of the respective contribution from either cell division or protein decay to loss of H2B-FP fluorescence in the most quiescent HSC subsets (i.e., RFP<sup>hi</sup> or GFP<sup>hi</sup>) remained challenging (Fig. 4 D). However, our finding of infrequent mitotic activity among primitive HSCs is well compatible with the experimental notion that HSCs are not required for steady-state hematopoiesis in adult mice (Schoedel et al., 2016; Sheikh et al., 2016). This is further supported by fate mapping experiments (Busch et al., 2015; Sun et al., 2014), which reported rare contribution of HSCs to adult steady-state hematopoiesis. Moreover, proliferation rates of primitive HSCs inferred from either BrdU uptake (1/55 d for HSC-1 [LSK CD48<sup>-/-</sup>CD150<sup>+</sup>CD229<sup>-/-</sup>CD244<sup>-</sup>]; Höfer et al., 2016; Oguro et al., 2013) or BrdU retention (1/145–193 d; van der Wath et al., 2009; Wilson et al., 2008) are in accordance with our conclusion that quiescent HSCs rarely but steadily divide as well as H2B-FP protein degradation being the major reason for loss of label over time in these cells.

We consistently estimated a proliferation rate of 1/23 d in actively cycling (RFP<sup>lo</sup> or GFP<sup>lo</sup>) LSK CD48<sup>-/-</sup>CD150<sup>+</sup> HSCs from both H2B-FP systems after correction for H2B-FP degradation, which is faster than the rate of 1/28–1/36 for “active” HSCs inferred from BrdU retention (van der Wath et al., 2009; Wilson et al., 2008). However, the latter studies identified immunophenotypic HSCs by exclusion of CD34<sup>+</sup> cells, a marker known to be up-regulated in proliferating HSCs (Sato et al., 1999). Our analysis of H2B-RFP retention in LSK CD48<sup>-/-</sup>CD150<sup>+</sup>CD34<sup>-/-</sup> cells revealed a division rate of 1/40 d for the proliferative RFP<sup>lo</sup> subpopulation (Fig. S3 C), which is highly similar to the division rate of active HSCs (van der Wath et al., 2009; Wilson et al., 2008) and substantiates our modeling approach. The division rates of proliferative HSCs (~1/8–1/18 d) and slowly cycling HSCs (~1/55–1/120 d) previously estimated from H2B-GFP retention data (Foudi et al., 2009) likely represent systematic overestimation due to neglect of label degradation. This illustrates the particular importance of considering label degradation in infrequently dividing cells.

In summary, H2B-FP transgenic models are important tools ideally suited to analyze and isolate viable cells based on differential mitotic activity. However, long-term tracing of discrete divisions of slowly cycling HSCs with label retention in the range of background fluorescence as performed by Bernitz et al. (2016) is not possible. The loss of label at early chase time points in these label retention experiments was mistakenly attributed to four discrete cell divisions, while our data strongly suggest that this loss of label largely represented protein degradation. At

longer chase intervals, accumulation of high background fluorescence was most likely misinterpreted as stable retention of previously pulsed label by Bernitz et al. (2016). Accounting for division-independent protein decay as well as for age-dependent background label accumulation is essential for estimating the divisional activity of rarely dividing cell populations in H2B-FP pulse-chase experiments. We found no evidence for abrupt entry into permanent quiescence or sudden loss of repopulation potential after four discrete self-renewal divisions of HSCs. We rather conclude from our data that primitive HSCs continue to cycle rarely in aged mice.

## Materials and methods

### Experimental model and subject details

#### Mice

R26<sup>rtTA</sup>/Col1A1<sup>H2B-RFP</sup> (Jax no. 014602; Egli et al., 2007) and R26<sup>rtTA</sup>/Col1A1<sup>H2B-GFP</sup> (Jax no. 016836; Foudi et al., 2009), C57Bl/6Jrj WT (Janvier), B6.CD45.1 (Jax no. 002014), B6CD45.1/-2, and Ki67-RFP (obtained from the Clevers laboratory, Hubrecht Institute, Utrecht, Netherlands; Basak et al., 2014) mice were housed at the Experimental Center, TU Dresden. Tg(tetO-HIST1H2Bj/GFP)47Efu/J (tetO-H2B-GFP47Efu/J) were imported from Jackson Laboratories (Jax no. 005104) and housed at the animal facility of the Biomedical Center, Lund University. Tg(tetO-HIST1H2Bj/GFP)47Efu mice were backcrossed to C57Bl/6 genetic background for >10 generations to yield the B6.tetO-H2B-GFP47Efu strain, which was housed at Deutsches Krebsforschungszentrum Heidelberg. Pulse-chase data of R26<sup>rtTA</sup>/Col1A1<sup>H2B-RFP</sup> mice were previously published (Morcos et al., 2017; Säwén et al., 2016).

H2B-FP mice were induced with DOX either via chow (Ssniff Spezialdiäten, 625 mg/kg for 10–11 wk or 2,000 mg/kg for either 3–7 wk [this study] or 1 wk [Säwén et al., 2016]) or via drinking water (1 mg/ml DOX [Applichem], 1% sucrose for 8 wk [Morcos et al., 2017]) ad libitum.

5-FU (150 µg/g body weight, Applichem) was administered via i.v. injection.

All animal experiments were in accordance with institutional guidelines and were approved by the relevant authorities (Landesdirektion Dresden, Regierungspräsidium Karlsruhe, and local ethics committee, University Lund).

### Methods details

#### Cell preparation

Whole BM cells (WBMCs) were isolated by crushing long bones with mortar and pestle using PBS/2% FCS/2 mM EDTA and filtered through a 100-µm mesh. After erythrocyte lysis in hypotonic NH<sub>4</sub>Cl<sup>-</sup>buffer, cells were filtered through a 40-µm mesh. Hematopoietic lineage<sup>+</sup> cells were removed with the lineage cell depletion kit (Miltenyi Biotec).

PB was drawn into glass capillaries by retrobulbar puncture. For chimerism analysis, blood was flushed out of the capillary using PBS/heparin (250 U/ml, Biochrom). Erythrocyte lysis in NH<sub>4</sub>Cl<sup>-</sup> buffer was performed twice for 5 min. For hemograms, blood was drawn by retrobulbar puncture directly into EDTA-coated tubes (Sarstedt) and analyzed on a XT-2000i Vet analyzer (Sysmex).



### BM transplantation

B6.CD45.1/2 recipient mice received a single dose of 9 Gray total body irradiation (Yxlon Maxi Shot  $\gamma$ -source). Donor cells (purified LSK CD48<sup>-/lo</sup>CD150<sup>+</sup> test cells mixed with B6.CD45.1 competitor WBMCs) were administered via intravenous injection into the retro-orbital sinus. For secondary transplantation, equal numbers of WBMCs from all primary transplanted individuals were pooled, and  $4 \times 10^6$  cells were transplanted into each lethally irradiated secondary recipients. Recipient PB T-lymphocytes (CD3<sup>+</sup>), B-lymphocytes (CD19<sup>+</sup>), and neutrophils (CD11b<sup>+</sup>, Gr-1<sup>hi</sup>) were analyzed for their donor origin using a MACSquant flow cytometer (Miltenyi).

### Flow cytometry

Cells were incubated with antibodies (Table S1) in PBS/2% FCS for 30 min, washed twice with PBS/2% FCS, and analyzed on an ARIA II SORP or ARIA III (BD Biosciences). H2B-FP fluorescence intensities from independent experiments on the same flow cytometer were normalized using Sphero Rainbow 8 peak particles (BD Bioscience) as reference. Data were analyzed with FlowJo V9.9 software (Tree Star), and gates were set according to Fluorescence-Minus-One controls. For a detailed overview of gating strategies, refer to Fig. S1 A.

### Single cell RNA sequencing

Single BM LSK CD48<sup>-/lo</sup>CD150<sup>+</sup> cells were index-sorted into 96-well plates containing 2  $\mu$ l of nuclease-free water with 0.2% Triton X-100 and 4 U murine RNase Inhibitor (NEB), spun down and frozen at  $-80^{\circ}\text{C}$ . After thawing, 2  $\mu$ l of a primer mix were added (5 mM deoxynucleoside triphosphates [Invitrogen], 0.5  $\mu$ M dT-primer [C6-aminolinker 5'-AAGCAGTGGTATCAACG-CAGAGTCGACTTTTTTTTTTTTTTTTTTTTTTTTTTTTTTTTTTTTTVN-3'], and 4 U RNase Inhibitor [NEB]). RNA was denatured for 3 min at  $72^{\circ}\text{C}$ , and the RT was performed at  $42^{\circ}\text{C}$  for 90 min after filling up to 10  $\mu$ l with RT buffer mix for a final concentration of 1 $\times$  superscript II buffer (Invitrogen), 1 M betaine, 5 mM dithiothreitol, 6 mM MgCl<sub>2</sub>, 1  $\mu$ M template switch oligo (5'-AAGCAGTGGTATCAACGCAGAGTACATrGrG-3'), 9 U RNase Inhibitor, and 90 U Superscript II (Invitrogen). After synthesis, the RT was inactivated at  $70^{\circ}\text{C}$  for 15 min. The cDNA was amplified using Kapa HiFi HotStart Readymix (Peqlab) at a final 1 $\times$  concentration and 0.1  $\mu$ M primer (5'-AAGCAGTGGTATCAACGCAGAGT-3') under the following cycling conditions: initial denaturation at  $98^{\circ}\text{C}$  for 3 min, 22 cycles ( $98^{\circ}\text{C}$  20 s,  $67^{\circ}\text{C}$  15 s,  $72^{\circ}\text{C}$  6 min), and final elongation at  $72^{\circ}\text{C}$  for 5 min. The amplified cDNA was purified using 1 $\times$  volume of hydrophobic Sera-Mag SpeedBeads (GE Healthcare), and DNA was eluted in 12  $\mu$ l nuclease-free water. The concentration of the samples was measured with a Tecan plate reader Infinite 200 pro in 384-well black flat-bottom low-volume plates (Corning) using AccuBlue Broad range chemistry (Biotium).

For library preparation, 700 pg cDNA in 2  $\mu$ l nuclease-free water was mixed with 0.5  $\mu$ l Tagment DNA Enzyme and 2.5  $\mu$ l Tagment DNA Buffer (Nextera, Illumina) and tagmented at  $55^{\circ}\text{C}$  for 5 min. Subsequently, Illumina indices were added during PCR ( $72^{\circ}\text{C}$  3 min,  $98^{\circ}\text{C}$  30 s, 12 cycles [ $98^{\circ}\text{C}$  10 s,  $63^{\circ}\text{C}$  20 s,  $72^{\circ}\text{C}$  1 min],  $72^{\circ}\text{C}$  5 min) with 1 $\times$  concentrated KAPA HiFi HotStart Ready Mix and 0.7  $\mu$ M dual indexing primers. After PCR,

libraries were quantified with AccuBlue Broad range chemistry, equimolarly pooled, and purified twice with 1 $\times$  volume Sera-Mag SpeedBeads. This was followed by Illumina single-end sequencing (76 bp) on a Nextseq550 aiming at an average sequencing depth of  $5 \times 10^5$  reads per cell. Raw sequencing data were submitted to the National Center for Biotechnology Information Gene Expression Omnibus under accession number GSE144987.

### Single-cell transcriptome analysis

Raw reads were mapped to the mouse genome (mm10) and splice-site information from Ensembl release 87 (Zerbino et al., 2018) with gsnap (version 2018-07-04; Wu and Nacu, 2010). Uniquely mapped reads and gene annotations from Ensembl were used as input for featureCounts (version 1.6.2; Liao et al., 2014) to create counts per gene and cell.

Further analysis of the single cell counts data were done with the R package scater (version 1.8.4; McCarthy et al., 2017). Cells that met one of the following criteria were considered low-quality: (1) total counts <5,000, (2) total genes <2,000 or >10,000, (3) percentage of counts from mitochondrial genes >6%, (4) percentage of counts from External RNA Controls Consortium spike-in transcripts >25%, and (5) percentage of genes without counts >95%. Consequently, 82 low-quality cells (29%) were removed. Also, genes that were expressed in less than one third of the remaining 200 cells were considered as low-expressed and removed, leaving 6,358 genes for further analysis.

For the filtered counts matrix (6,358 genes  $\times$  200 cells), counts per million normalization was applied to alleviate the effect of different sequencing depth across the cells. To make expression values comparable, expression values of a gene were transformed to the scale [0,1] where 0 was the minimum and 1 the maximum counts per million value of this gene across cells.

Gene signature of quiescent HSCs (MoIO) and gene signature of proliferative HSCs (NoMO) genes (Wilson et al., 2015), which showed expression in our data, were considered (18 and 15 genes, respectively). The scores were then calculated by averaging the normalized scaled expression values of MoIO and NoMO gene sets, respectively. The relationship between fluorescence markers (H2B-GFP and Sca-1, in logarithmic scale), and MoIO/NoMO scores was calculated using linear regression.

To identify functional changes in gene expression correlated with H2B-GFP marker expression, for each gene, its Spearman correlation coefficient to the fluorescence marker (H2B-GFP and Sca-1) was calculated. The top 100 positive and top 100 negative correlated genes were analyzed for associated terms from the Gene Ontology database, aspect Biological Process using DAVID 6.8 (Huang et al., 2009). Very broad and unspecific Gene Ontology Biological Process terms were excluded by the FAT filter, similar/redundant terms were grouped into annotation clusters, and enrichment scores were calculated. All clusters with an enrichment score >1 were considered.

### Mathematical modeling

The dilution kinetics of the fluorescent H2B-FP is formulated in terms of an ordinary differential equation describing the

average kinetics of the amount of label, termed  $X$ , in a homogeneous population:

$$\frac{dX}{dt} = -(\lambda_1 + \lambda_2) \cdot X + b,$$

with (i) the rate of permanent leaky background FP production  $b$ , (ii) FP decay due to division with a rate  $\lambda_1$ , and (iii) division-independent FP decay due to protein degradation with a rate  $\lambda_2$ . The initial condition  $X(0) = a$  describes the induced amount of FP label  $a$  in case of an H2B-FP induction. This model assumes a homogeneous population constant in size. This means that cell differentiation balances the increase by cell division, and differentiating cells are no longer considered as part of the modeled HSC population. Cell cycle times are assumed to follow an exponential distribution with mean  $1/\lambda_1$ . There is no memory or heritability in the process: the probability of a cell to divide does not depend on former divisions. Furthermore, the probability of differentiation (and subsequent extinction from the stem cell compartment) does not depend on the number of cell divisions that a cell has undergone.

The equation can be solved explicitly to

$$X(t) = a \cdot e^{-(\lambda_1 + \lambda_2)t} + (1 - e^{-(\lambda_1 + \lambda_2)t}) \cdot \frac{b}{\lambda_1 + \lambda_2}$$

and was fitted to the logarithmic data using the nonlinear model fit routine in Mathematica (version 11.3).

In the long run, the system reaches a steady-state (i.e., a protein level that does not change over time) at  $b/(\lambda_1 + \lambda_2)$ , independent of the initially provided amount of label  $a$ . At this equilibrium level, leaky background production (described by  $b$ ) and decay due to cell division and protein degradation (described by  $\lambda_1 + \lambda_2$ ) are leveling out. This model describes the average kinetics of a homogeneous population. It thus assumes that all cells in this population have the same rate  $b$  of leaky background production as well as homogenous degradation of H2B-FP.

To determine the time until chased and background control populations merge (Fig. S4 B), we assume that the chase period starts at 10 wk after birth, while the background accumulation is assumed to start at 4 wk after birth when the adult hematopoiesis is established (Bowie et al., 2006), thus leading to a time shift between both populations of 6 wk (42 d). We define the time point of merging as the time when the chased population reaches at least 95% of the background control population. Assuming the limiting case of no cell division, this leads to the following equation:

$$0.95 \cdot \left( a \cdot e^{-\lambda_2 t} + (1 - e^{-\lambda_2 t}) \cdot \frac{b}{\lambda_2} \right) = (1 - e^{-\lambda_2(t+42)}) \cdot \frac{b}{\lambda_2},$$

which resolves to

$$t = \frac{1}{\lambda} \cdot \ln \left( 20 \cdot e^{-42\lambda_2} + 19 \cdot \frac{a\lambda_2 - b}{b} \right).$$

To study the process of establishing a stable level of H2B-FP background after birth (Fig. 3 A), a model comprised of two independent HSC populations was used based on the following assumptions: (i) The initial level of label at the time point of 4 wk

is assumed to be autofluorescence. This assumes that juvenile HSC cycle fast and thus do not or neglectably accumulate H2B-FP label until the hematopoietic system is established. (ii) We assume a mixture of two HSC populations: a proliferative population (90%) with an average cycling of 16 d and a quiescent population (10%) that does not cycle. (iii) For H2B-FP degradation, we assume a half-life of 2 wk for H2B-RFP and 6 wk for H2B-GFP as estimated.

To estimate subpopulations from H2B-FP distributions (Fig. 4), a mixture distribution of up to four normal distributions was fitted to the logarithmic data. Estimated subpopulation means were then separately fitted by the mathematical model.

### Quantification and statistical analyses

Data are presented as mean and SD. Statistical analysis was done with Prism 5 (Graphpad), and applied statistical tests are denominated in the respective figure legends. Significant results are indicated by \*,  $P = 0.01-0.05$ , \*\*,  $P = 0.001-0.01$ , and \*\*\*,  $P < 0.001$ ; nonsignificant results are indicated by ns.

### Online supplemental material

Fig. S1 presents additional data on H2B-FP background accumulation in primitive HSPCs. Fig. S2 displays the quiescence-related gene signatures and repopulation potential of HSCs accumulating high levels of H2B-FP background. Fig. S3 provides representative examples of H2B-FP dilution after different chase intervals. Fig. S4 shows simulations of H2B-FP pulse-chase experiments and data on labeling homogeneity. Table S1 lists antibody conjugates used for flow cytometry.

### Acknowledgments

We thank Livia Schulze, Tobias Häring, Christina Hiller, and Christa Haase for technical assistance, Jeffrey Bernitz for scientific discussions, and Thomas Höfer and Kristina Schödel for critical reading of the manuscript.

A. Gerbaulet was supported by the German Research Council (DFG, GE3038/1-1). Y. Ge and A. Roers were funded by the German Research Council (RO2133/10-1) in the setting of FOR2577. M.N.F. Morcos was supported by the Dresden International Graduate School for Biomedicine and Bioengineering, granted by the German Research Council in the context of the Excellence Initiative. The work of T. Zerjatke and I. Glauche was supported by the German Federal Ministry of Education and Research, grant O31A315 “MessAge” to I. Glauche. P. Säwén, H. Wan, and D. Bryder acknowledge funding from the Tobias Foundation and the Swedish Cancer Society.

Author contributions: M.N.F. Morcos, C.M. Munz, and A. Gerbaulet designed, performed, and analyzed experiments. M.N.F. Morcos, A. Gerbaulet, T. Zerjatke, and I. Glauche conceptualized data analysis. T. Zerjatke and I. Glauche conceived mathematical modeling. T. Zerjatke performed quantitative data analysis and implemented the mathematical modeling. Y. Ge, A. Petzold, S. Reinhardt, and A. Dahl performed transcriptome analysis. P. Säwén, H. Wan, D. Bryder, N.S. Anstee, R. Bogeska, and M.D. Milsom provided H2B-FP data. A. Gerbaulet conceived and supervised the study and wrote the manuscript. A. Roers

advised the study and edited the manuscript. All authors read, commented, and agreed on the final version of the manuscript.

Disclosures: The authors declare no competing interests exist.

Submitted: 16 July 2019

Revised: 23 August 2019

Accepted: 4 March 2020

## References

- Basak, O., M. van de Born, J. Korving, J. Beumer, S. van der Elst, J.H. van Es, and H. Clevers. 2014. Mapping early fate determination in *Igr5+* crypt stem cells using a novel *Ki67-RFP* allele. *EMBO J.* 33:2057–2068. <https://doi.org/10.15252/embj.201488017>
- Beard, C., K. Hochedlinger, K. Plath, A. Wutz, and R. Jaenisch. 2006. Efficient method to generate single-copy transgenic mice by site-specific integration in embryonic stem cells. *Genesis.* 44:23–28. <https://doi.org/10.1002/gene.20180>
- Beerman, I., D. Bhattacharya, S. Zandi, M. Sigvardsson, I.L. Weissman, D. Bryder, and D.J. Rossi. 2010. Functionally distinct hematopoietic stem cells modulate hematopoietic lineage potential during aging by a mechanism of clonal expansion. *Proc. Natl. Acad. Sci. USA.* 107:5465–5470. <https://doi.org/10.1073/pnas.1000834107>
- Bernitz, J.M., H.S. Kim, B. MacArthur, H. Sieburg, and K. Moore. 2016. Hematopoietic Stem Cells Count and Remember Self-Renewal Divisions. *Cell.* 167:1296–1309.e10. <https://doi.org/10.1016/j.cell.2016.10.022>
- Bowie, M.B., K.D. McKnight, D.G. Kent, L. McCaffrey, P.A. Hoodless, and C.J. Eaves. 2006. Hematopoietic stem cells proliferate until after birth and show a reversible phase-specific engraftment defect. *J. Clin. Invest.* 116:2808–2816. <https://doi.org/10.1172/JCI28310>
- Busch, K., K. Klapproth, M. Barile, M. Flossdorf, T. Holland-Letz, S.M. Schlenner, M. Reth, T. Höfer, and H.-R. Rodewald. 2015. Fundamental properties of unperturbed haematopoiesis from stem cells in vivo. *Nature.* 518:542–546. <https://doi.org/10.1038/nature14242>
- Challen, G.A., and M.A. Goodell. 2008. Promiscuous expression of H2B-GFP transgene in hematopoietic stem cells. *PLoS One.* 3:e2357. <https://doi.org/10.1371/journal.pone.0002357>
- Eaves, C.J. 2015. Hematopoietic stem cells: concepts, definitions, and the new reality. *Blood.* 125:2605–2613. <https://doi.org/10.1182/blood-2014-12-570200>
- Egli, D., J. Rosains, G. Birkhoff, and K. Eggan. 2007. Developmental reprogramming after chromosome transfer into mitotic mouse zygotes. *Nature.* 447:679–685. <https://doi.org/10.1038/nature05879>
- Fleming, W.H., E.J. Alpern, N. Uchida, K. Ikuta, G.J. Spangrude, and I.L. Weissman. 1993. Functional heterogeneity is associated with the cell cycle status of murine hematopoietic stem cells. *J. Cell Biol.* 122:897–902. <https://doi.org/10.1083/jcb.122.4.897>
- Foudi, A., K. Hochedlinger, D. Van Buren, J.W. Schindler, R. Jaenisch, V. Carey, and H. Hock. 2009. Analysis of histone 2B-GFP retention reveals slowly cycling hematopoietic stem cells. *Nat. Biotechnol.* 27:84–90. <https://doi.org/10.1038/nbt.1517>
- Glauche, I., K. Moore, L. Thielecke, K. Horn, M. Loeffler, and I. Roeder. 2009. Stem cell proliferation and quiescence—two sides of the same coin. *PLoS Comput. Biol.* 5:e1000447. <https://doi.org/10.1371/journal.pcbi.1000447>
- Gossen, M., and H. Bujard. 2002. Studying gene function in eukaryotes by conditional gene inactivation. *Annu. Rev. Genet.* 36:153–173. <https://doi.org/10.1146/annurev.genet.36.041002.120114>
- Grinenko, T., K. Arndt, M. Portz, N. Mende, M. Günther, K.N. Cosgun, D. Alexopoulou, N. Lakshmanaperumal, I. Henry, A. Dahl, and C. Waskow. 2014. Clonal expansion capacity defines two consecutive developmental stages of long-term hematopoietic stem cells. *J. Exp. Med.* 211:209–215. <https://doi.org/10.1084/jem.20131115>
- Harrison, D.E., and C.P. Lerner. 1991. Most primitive hematopoietic stem cells are stimulated to cycle rapidly after treatment with 5-fluorouracil. *Blood.* 78:1237–1240. <https://doi.org/10.1182/blood.V78.5.1237.1237>
- Höfer, T., K. Busch, K. Klapproth, and H.-R. Rodewald. 2016. Fate Mapping and Quantitation of Hematopoiesis In Vivo. *Annu. Rev. Immunol.* 34:449–478. <https://doi.org/10.1146/annurev-immunol-032414-112019>
- Huang, W., B.T. Sherman, and R.A. Lempicki. 2009. Systematic and integrative analysis of large gene lists using DAVID bioinformatics resources. *Nat. Protoc.* 4:44–57. <https://doi.org/10.1038/nprot.2008.211>
- Jamai, A., R.M. Imoberdorf, and M. Strubin. 2007. Continuous histone H2B and transcription-dependent histone H3 exchange in yeast cells outside of replication. *Mol. Cell.* 25:345–355. <https://doi.org/10.1016/j.molcel.2007.01.019>
- Kanda, T., K.F. Sullivan, and G.M. Wahl. 1998. Histone-GFP fusion protein enables sensitive analysis of chromosome dynamics in living mammalian cells. *Curr. Biol.* 8:377–385. [https://doi.org/10.1016/S0960-9822\(98\)70156-3](https://doi.org/10.1016/S0960-9822(98)70156-3)
- Kent, D.G., M.R. Copley, C. Benz, S. Wöhrer, B.J. Dykstra, E. Ma, J. Cheyne, Y. Zhao, M.B. Bowie, Y. Zhao, et al. 2009. Prospective isolation and molecular characterization of hematopoietic stem cells with durable self-renewal potential. *Blood.* 113:6342–6350. <https://doi.org/10.1182/blood-2008-12-192054>
- Kiel, M.J., Ö.H. Yilmaz, T. Iwashita, Ö.H. Yilmaz, C. Terhorst, and S.J. Morrison. 2005. SLAM family receptors distinguish hematopoietic stem and progenitor cells and reveal endothelial niches for stem cells. *Cell.* 121:1109–1121. <https://doi.org/10.1016/j.cell.2005.05.026>
- Kiel, M.J., S. He, R. Ashkenazi, S.N. Gentry, M. Teta, J.A. Kushner, T.L. Jackson, and S.J. Morrison. 2007. Haematopoietic stem cells do not asymmetrically segregate chromosomes or retain BrdU. *Nature.* 449:238–242. <https://doi.org/10.1038/nature06115>
- Kimura, H., and P.R. Cook. 2001. Kinetics of core histones in living human cells: little exchange of H3 and H4 and some rapid exchange of H2B. *J. Cell Biol.* 153:1341–1353. <https://doi.org/10.1083/jcb.153.7.1341>
- Li, Q., N. Bohin, T. Wen, V. Ng, J. Magee, S.-C. Chen, K. Shannon, and S.J. Morrison. 2013. Oncogenic Nras has bimodal effects on stem cells that sustainably increase competitiveness. *Nature.* 504:143–147. <https://doi.org/10.1038/nature12830>
- Liao, Y., G.K. Smyth, and W. Shi. 2014. featureCounts: an efficient general purpose program for assigning sequence reads to genomic features. *Bioinformatics.* 30:923–930. <https://doi.org/10.1093/bioinformatics/btt656>
- McCarthy, D.J., K.R. Campbell, A.T.L. Lun, and Q.F. Wills. 2017. Scater: pre-processing, quality control, normalization and visualization of single-cell RNA-seq data in R. *Bioinformatics.* 33:1179–1186.
- Morcos, M.N.F., K.B. Schoedel, A. Hoppe, R. Behrendt, O. Basak, H.C. Clevers, A. Roers, and A. Gerbaulet. 2017. SCA-1 Expression Level Identifies Quiescent Hematopoietic Stem and Progenitor Cells. *Stem Cell Reports.* 8:1472–1478. <https://doi.org/10.1016/j.stemcr.2017.04.012>
- Nakada, D., H. Oguro, B.P. Levi, N. Ryan, A. Kitano, Y. Saitoh, M. Takeichi, G.R. Wendt, and S.J. Morrison. 2014. Oestrogen increases haematopoietic stem-cell self-renewal in females and during pregnancy. *Nature.* 505:555–558. <https://doi.org/10.1038/nature12932>
- Oguro, H., L. Ding, and S.J. Morrison. 2013. SLAM family markers resolve functionally distinct subpopulations of hematopoietic stem cells and multipotent progenitors. *Cell Stem Cell.* 13:102–116. <https://doi.org/10.1016/j.stem.2013.05.014>
- Osawa, M., K. Hanada, H. Hamada, and H. Nakauchi. 1996. Long-term lymphohematopoietic reconstitution by a single CD34-low/negative hematopoietic stem cell. *Science.* 273:242–245. <https://doi.org/10.1126/science.273.5272.242>
- Passegué, E., A.J. Wagers, S. Giuriato, W.C. Anderson, and I.L. Weissman. 2005. Global analysis of proliferation and cell cycle gene expression in the regulation of hematopoietic stem and progenitor cell fates. *J. Exp. Med.* 202:1599–1611. <https://doi.org/10.1084/jem.20050967>
- Qiu, J., D. Papatsenko, X. Niu, C. Schaniel, and K. Moore. 2014. Divisional history and hematopoietic stem cell function during homeostasis. *Stem Cell Reports.* 2:473–490. <https://doi.org/10.1016/j.stemcr.2014.01.016>
- Radomska, H.S., D.A. Gonzalez, Y. Okuno, H. Iwasaki, A. Nagy, K. Akashi, D.G. Tenen, and C.S. Huettnner. 2002. Transgenic targeting with regulatory elements of the human CD34 gene. *Blood.* 100:4410–4419. <https://doi.org/10.1182/blood-2002-02-0355>
- Sato, T., J.H. Laver, and M. Ogawa. 1999. Reversible expression of CD34 by murine hematopoietic stem cells. *Blood.* 94:2548–2554. [https://doi.org/10.1182/blood.V94.8.2548.420k38\\_2548\\_2554](https://doi.org/10.1182/blood.V94.8.2548.420k38_2548_2554)
- Såwén, P., S. Lang, P. Mandal, D.J. Rossi, S. Soneji, and D. Bryder. 2016. Mitotic History Reveals Distinct Stem Cell Populations and Their Contributions to Hematopoiesis. *Cell Rep.* 14:2809–2818. <https://doi.org/10.1016/j.celrep.2016.02.073>
- Schoedel, K., M. Morcos, T. Zerjatke, I. Roeder, T. Grinenko, D. Voehringer, J. Göthert, C. Waskow, A. Roers, and A. Gerbaulet. 2016. The bulk of the hematopoietic stem cell population is dispensable for murine steady-state and stress hematopoiesis. *Blood.* 128:2285–2296. <https://doi.org/10.1182/blood-2016-03-706010>
- Sheikh, B.N., Y. Yang, J. Schreuder, S.K. Nilsson, R. Bilardi, S. Carotta, H.M. McRae, D. Metcalf, A.K. Voss, and T. Thomas. 2016. MOZ (KAT6A) is

- essential for the maintenance of classically defined adult hematopoietic stem cells. *Blood*. 128:2307–2318. <https://doi.org/10.1182/blood-2015-10-676072>
- Shin, J.Y., W. Hu, M. Naramura, and C.Y. Park. 2014. High c-Kit expression identifies hematopoietic stem cells with impaired self-renewal and megakaryocytic bias. *J. Exp. Med.* 211:217–231. <https://doi.org/10.1084/jem.20131128>
- Spangrude, G.J., and G.R. Johnson. 1990. Resting and activated subsets of mouse multipotent hematopoietic stem cells. *Proc. Natl. Acad. Sci. USA*. 87:7433–7437. <https://doi.org/10.1073/pnas.87.19.7433>
- Sun, J., A. Ramos, B. Chapman, J.B. Johnnidis, L. Le, Y.-J. Ho, A. Klein, O. Hofmann, and F.D. Camargo. 2014. Clonal dynamics of native haematopoiesis. *Nature*. 514:322–327. <https://doi.org/10.1038/nature13824>
- Takizawa, H., R.R. Regoes, C.S. Boddupalli, S. Bonhoeffer, and M.G. Manz. 2011. Dynamic variation in cycling of hematopoietic stem cells in steady state and inflammation. *J. Exp. Med.* 208:273–284. <https://doi.org/10.1084/jem.20101643>
- Toyama, B.H., J.N. Savas, S.K. Park, M.S. Harris, N.T. Ingolia, J.R. Yates III, and M.W. Hetzer. 2013. Identification of long-lived proteins reveals exceptional stability of essential cellular structures. *Cell*. 154:971–982. <https://doi.org/10.1016/j.cell.2013.07.037>
- Tumbar, T., G. Guasch, V. Greco, C. Blanpain, W.E. Lowry, M. Rendl, and E. Fuchs. 2004. Defining the epithelial stem cell niche in skin. *Science*. 303:359–363. <https://doi.org/10.1126/science.1092436>
- van der Wath, R.C., A. Wilson, E. Laurenti, A. Trumpp, and P. Liò. 2009. Estimating dormant and active hematopoietic stem cell kinetics through extensive modeling of bromodeoxyuridine label-retaining cell dynamics. *PLoS One*. 4:e6972. <https://doi.org/10.1371/journal.pone.0006972>
- Venkatesh, S., and J.L. Workman. 2015. Histone exchange, chromatin structure and the regulation of transcription. *Nat. Rev. Mol. Cell Biol.* 16:178–189. <https://doi.org/10.1038/nrm3941>
- Waghmare, S.K., R. Bansal, J. Lee, Y.V. Zhang, D.J. McDermitt, and T. Tumbar. 2008. Quantitative proliferation dynamics and random chromosome segregation of hair follicle stem cells. *EMBO J.* 27:1309–1320. <https://doi.org/10.1038/emboj.2008.72>
- Wilson, A., E. Laurenti, G. Oser, R.C. van der Wath, W. Blanco-Bose, M. Jaworski, S. Offner, C.F. Dunant, L. Eshkind, E. Bockamp, et al. 2008. Hematopoietic stem cells reversibly switch from dormancy to self-renewal during homeostasis and repair. *Cell*. 135:1118–1129. <https://doi.org/10.1016/j.cell.2008.10.048>
- Wilson, N.K., D.G. Kent, F. Buettner, M. Shehata, I.C. Macaulay, F.J. Calero-Nieto, M. Sánchez Castillo, C.A. Oedekoven, E. Diamanti, R. Schulte, et al. 2015. Combined Single-Cell Functional and Gene Expression Analysis Resolves Heterogeneity within Stem Cell Populations. *Cell Stem Cell*. 16:712–724. <https://doi.org/10.1016/j.stem.2015.04.004>
- Wu, T.D., and S. Nacu. 2010. Fast and SNP-tolerant detection of complex variants and splicing in short reads. *Bioinformatics*. 26:873–881. <https://doi.org/10.1093/bioinformatics/btq057>
- Zerbino, D.R., P. Achuthan, W. Akanni, M.R. Amode, D. Barrell, J. Bhai, K. Billis, C. Cummins, A. Gall, C.G. Girón, et al. 2018. Ensembl 2018. *Nucleic Acids Res.* 46(D1):D754–D761. <https://doi.org/10.1093/nar/gkx1098>

## Supplemental material

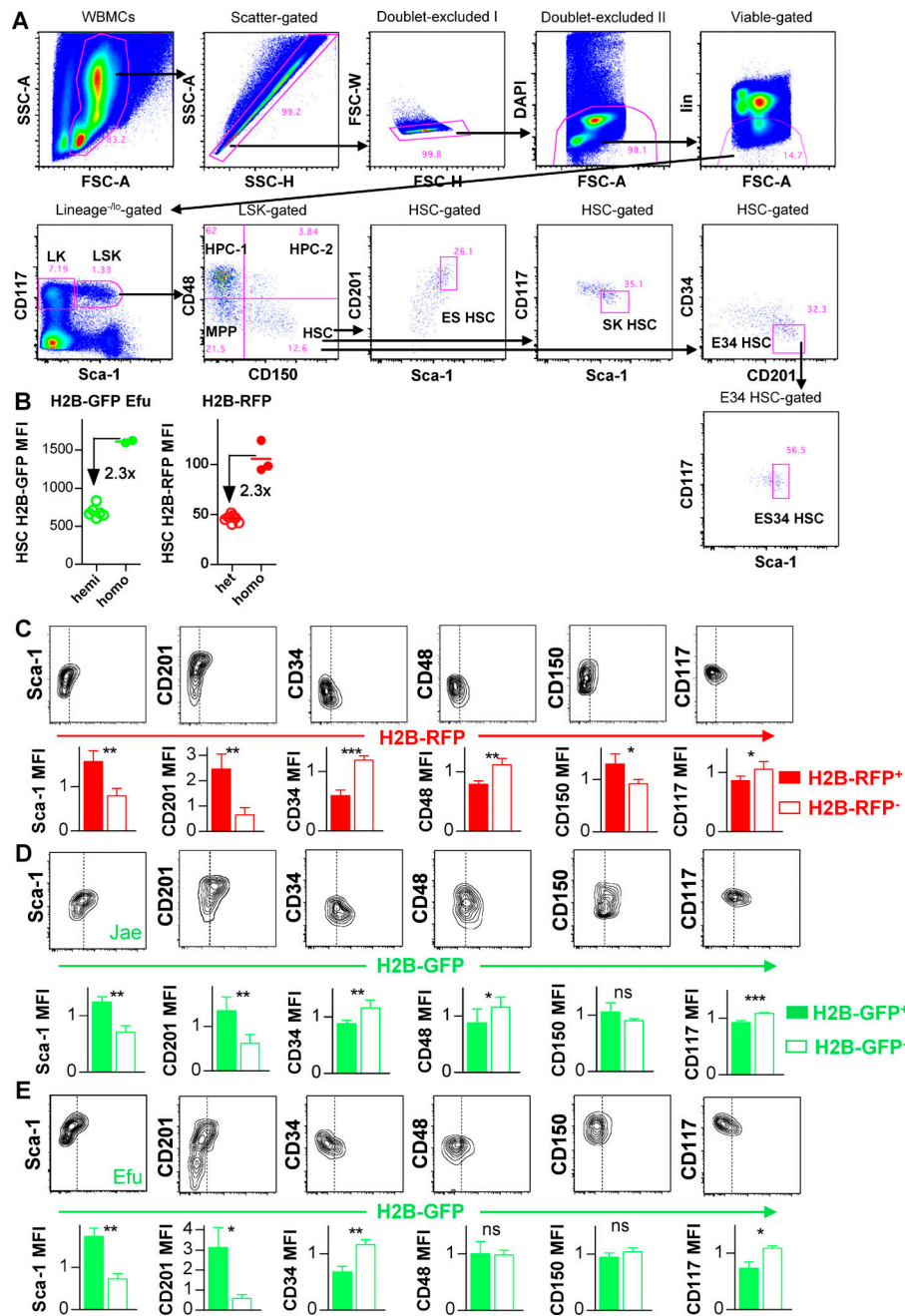


**Figure S1. Primitive HSPCs exhibit higher levels of leaky H2B-FP background fluorescence.** (A) Representative gating strategy of B6 WT HSPCs (LK:  $lin^{-/lo}Sca-1^{-}CD117^{+}$ ; LSK:  $lin^{-/lo}Sca-1^{+}CD117^{+}$ ; HPC-1: LSK  $CD48^{hi}CD150^{-}$ ; HPC-2: LSK  $CD48^{hi}CD150^{+}$ ; MPP: LSK  $CD48^{-/lo}CD150^{-}$ ; HSC: LSK  $CD48^{-/lo}CD150^{+}$ ; E34 HSC: LSK  $CD48^{-/lo}CD150^{+}CD34^{-/lo}CD201^{hi}$ ; ES34 HSC:  $LSK^{hi}K CD48^{-/lo}CD150^{+}CD34^{-/lo}CD201^{hi}$ ; SK HSC:  $LSK^{hi}K^{lo} CD48^{-/lo}CD150^{+}$ ; ES HSC:  $LSK^{hi}K CD48^{-/lo}CD150^{+}CD201^{hi}$ ). FSC, forward scatter; SSC, side scatter; lin, hematopoietic lineage antigens. (B) Age-matched hemi- ( $n = 6$ ) or homozygous ( $n = 2$ ) single transgenic tetO-H2B-GFP47Efu) as well as un-induced  $R26^{rtTA}/Col1A1^{H2B-RFP/wt}$  ( $n = 9$ , heterozygous) or  $R26^{rtTA}/Col1A1^{H2B-RFP/H2B-RFP}$  ( $n = 3$ , homozygous) mice were analyzed for H2B-FP MFI of HSCs (individuals and means [bars] are shown; fold of fluorescence reduction was calculated). (C-E) BM HSCs from repressed H2B-FPs transgenic mouse models were analyzed for background fluorescence and surface marker expression by flow cytometry. H2B-FP fluorescence of HSCs (LSK  $CD48^{-/lo}CD150^{+}$ ) in relation to surface markers is depicted (representative contour plots upper rows, dotted lines show gating threshold for events which are within  $[H2B-FP^{-}]$  or above  $[H2B-FP^{+}]$  autofluorescence). Lower rows: Comparison of surface marker expression between H2B-FP $^{-}$  and H2B-FP $^{+}$  HSCs (means and SD are shown, each surface marker expression was normalized to the respective mean MFI of the total HSC population). Significance was calculated by paired Student's *t* test. (C) BM HSCs of un-induced  $R26^{rtTA/wt}/Col1A1^{H2B-RFP/wt}$  mice ( $n = 4$ , representative of five independent experiments, aged 9–12 wk) mice were analyzed for H2B-RFP background fluorescence and surface marker expression. (D) BM HSCs of un-induced  $R26^{rtTA/rtTA}/Col1A1^{H2B-GFP/H2B-GFP}$  mice ( $n = 4$ , representative of five independent experiments, age 22 wk) mice were analyzed for H2B-GFP background fluorescence and surface marker expression. (E) BM HSCs of hemizygous, single transgenic B6.tetO-H2B-GFP47Efu mice ( $n = 3$ , pooled from three independent experiments, age 11–15 wk) were analyzed for H2B-GFP background fluorescence and surface marker expression. \*,  $P = 0.01-0.05$ ; \*\*,  $P = 0.001-0.01$ ; \*\*\*,  $P < 0.001$ ; ns, not significant.

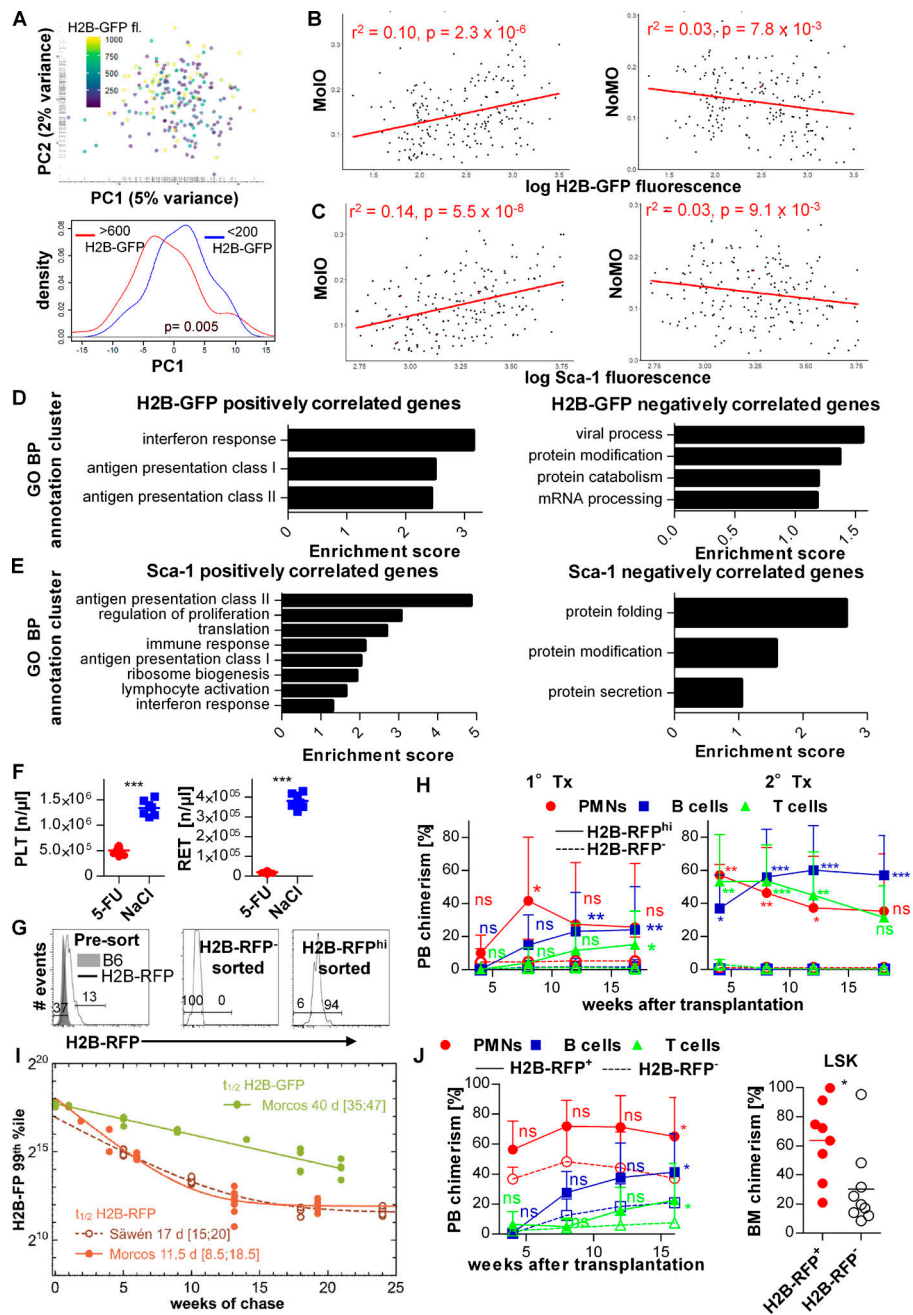


**Figure S2. HSCs retaining high levels of leaky H2B-FP background fluorescence express quiescence-related gene signature and exhibit high re-population potential.** **(A)** Principal component (PC) analysis of 200 index-sorted single HSCs (LSK CD48<sup>-/lo</sup>CD150<sup>+</sup>) isolated from un-induced *R26<sup>rtTA/rtTA</sup>/Col1A1<sup>H2B-GFP/H2B-GFP</sup>* mice ( $n = 6$ , aged 12–22 wk, data derived from two independent experiments) revealed separation of cells with high H2B-GFP background fluorescence (upper panel). Each cell was colored according to its H2B-GFP background fluorescence intensity (H2B-GFP fl), which was recorded during index-sorting. PC1 distributions of cells (lower panel) expressing either >600 (red histogram) or <200 (blue histogram) units of H2B-GFP fluorescence reveal significant (Mann–Whitney  $U$  test) enrichment of cells with high H2B-GFP background fluorescence in the left area of the PC analysis plot. **(B and C)** The recorded H2B-GFP (B) or Sca-1 (C) fluorescence of each single cell was correlated to normalized gene signatures of quiescent (MoLO, Wilson et al., 2015) or proliferative (NoMO) HSCs and revealed a significant positive correlation of H2B-GFP background fluorescence as well as Sca-1 surface expression to the MoLO score and concordant negative correlations to the NoMO score ( $r^2$  and significance was calculated by linear regression and F-test, respectively). The previously published (Wilson et al., 2015) correlations between the surface marker Sca-1 and the MoLO and NoMO signatures had similar direction, strength and significance in our dataset as the correlation of H2B-GFP background fluorescence to these gene signatures. **(D and E)** Plots show biological processes (BP) that are enriched in the first 100 genes positively (left panel) or negatively (right panel) correlated to either H2B-GFP background fluorescence (D) or Sca-1 surface expression (E). TOP100-negatively correlated genes were enriched for genes related to transcription and translation. Analysis was performed using the gene ontology (GO) BP database of DAVID 6.8. Similar terms were clustered, and enrichment scores (>1, log transformation of the DAVID Expression Analysis Systematic Explorer score) were calculated to determine overrepresentation of particular biological processes. **(F)** PB platelet (PLT) and reticulocyte (RET) counts of repressed *R26<sup>rtTA/rtTA</sup>/Col1A1<sup>H2B-GFP/H2B-GFP</sup>* mice were determined 6 d after 5-FU or saline injection (NaCl). **(G)** Sorting strategy (left histogram) for isolation and re-analysis (right histograms) of H2B-RFP<sup>-</sup> (middle) and H2B-RFP<sup>hi</sup> (right) HSCs (LSK CD48<sup>-/lo</sup>CD150<sup>+</sup>) from un-induced *R26<sup>rtTA/wt</sup>/Col1A1<sup>H2B-RFP/wt</sup>* (H2B-RFP) donor mice ( $n = 4$ ) is depicted. H2B-RFP<sup>-</sup> gate was set according to the red autofluorescence of B6 WT HSCs. The event frequency in each gate is shown. **(H)** 30 H2B-RFP<sup>-</sup> or H2B-RFP<sup>hi</sup> HSCs were purified from un-induced *R26<sup>rtTA/wt</sup>/Col1A1<sup>H2B-RFP/wt</sup>* animals ( $n = 6$ , 16–17 wk) and transplanted together with  $2 \times 10^5$  B6.CD45.1 WBMCS into irradiated B6.CD45.1/2 recipient mice ( $n = 9$  or 10 / per group). PB neutrophils (PMN, CD11b<sup>+</sup>Gr-1<sup>hi</sup>), B- (CD19<sup>+</sup>) and T-lymphocytes (CD3<sup>+</sup>) of primary recipients were analyzed for donor origin at indicated time points (left panel).  $4 \times 10^6$  WBMCS were secondary transplanted 17 wk after primary transplantation. PB neutrophils (PMN, CD11b<sup>+</sup>Gr-1<sup>hi</sup>), B- (CD19<sup>+</sup>) and T-lymphocytes (CD3<sup>+</sup>) of secondary recipients ( $n = 4$ /group) were analyzed for donor origin at indicated time points (right panel, mean and SD are shown, significance was calculated by repeated measures two-way ANOVA with Bonferroni post-test). **(I)** Maximum H2B-FP fluorescence intensities (as judged by the 99th percentile) of MPPs (LSK CD48<sup>-/lo</sup>CD150<sup>-</sup>) isolated from chased *R26<sup>rtTA</sup>/Col1A1<sup>H2B-RFP</sup>* (shown in red; Säwén et al., 2016, dashed line, open circles; Morcos et al., 2017, continuous line, filled circles) or *R26<sup>rtTA/rtTA</sup>/Col1A1<sup>H2B-GFP/H2B-GFP</sup>* (green; same animals as in Fig. 2 A “GFP Morcos”) individual mice are depicted. H2B-FP half-lives and respective 95% confidence intervals (squared brackets) were calculated. **(J)** Competitive transplantation of *R26<sup>rtTA/wt</sup>/Col1A1<sup>H2B-RFP/wt</sup>* animals after the second chase (Fig. 2 F). 200 H2B-RFP<sup>+</sup> (continuous lines) or H2B-RFP<sup>-</sup> (dotted lines) HSCs were purified, mixed with  $3 \times 10^5$  B6.CD45.1 WBMCS, and each transplanted into lethally irradiated WT recipients ( $n = 8$  or 9/ donor cell type). PB neutrophil, B and T cell chimerism was analyzed for 16 wk (left, significance was calculated by repeated measures two-way ANOVA with Bonferroni post-test). BM LSK chimerism was analyzed after 17 wk (right panel, individual recipient mice and means are shown, significance was calculated by an un-paired Student’s  $t$  test). \*,  $P = 0.01–0.05$ ; \*\*,  $P = 0.001–0.01$ ; \*\*\*,  $P < 0.001$ ; ns, not significant.



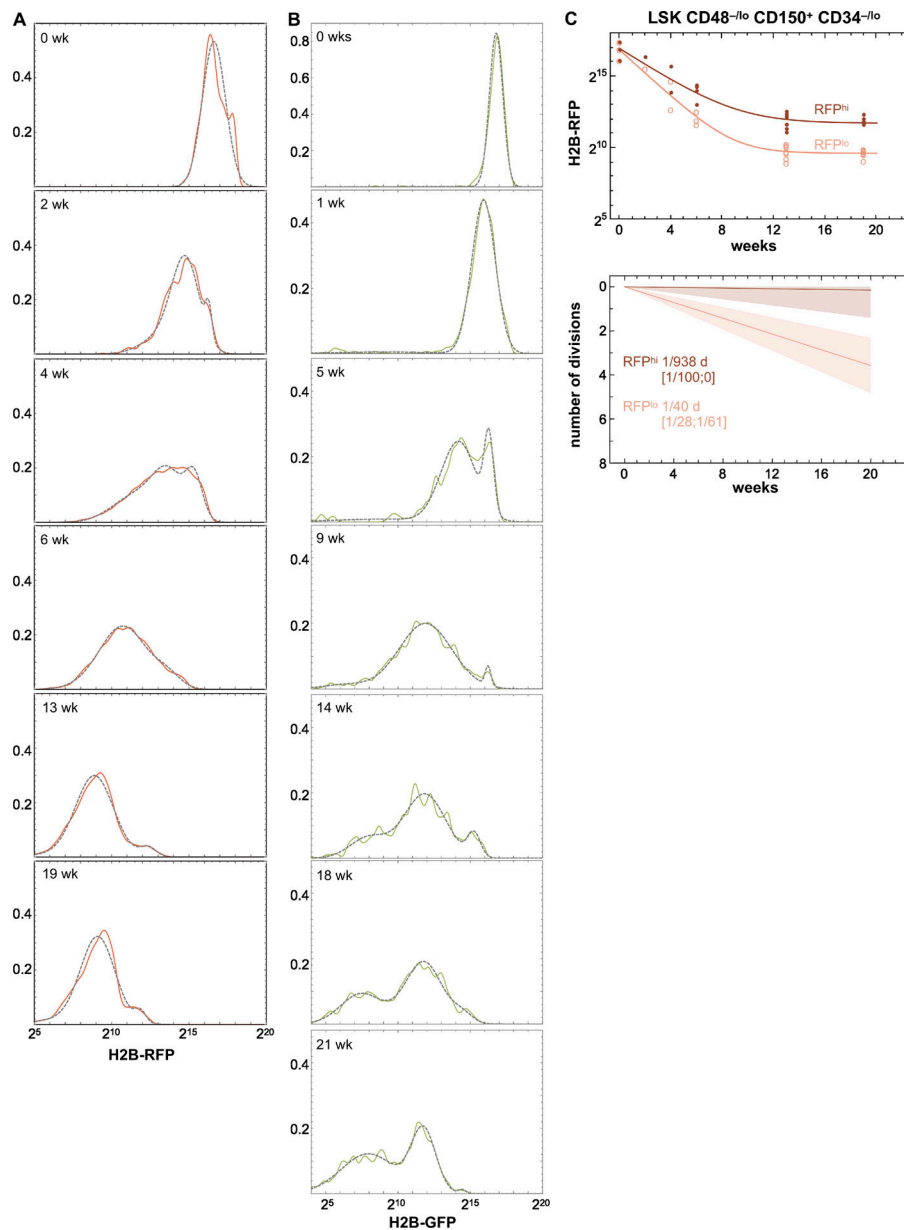
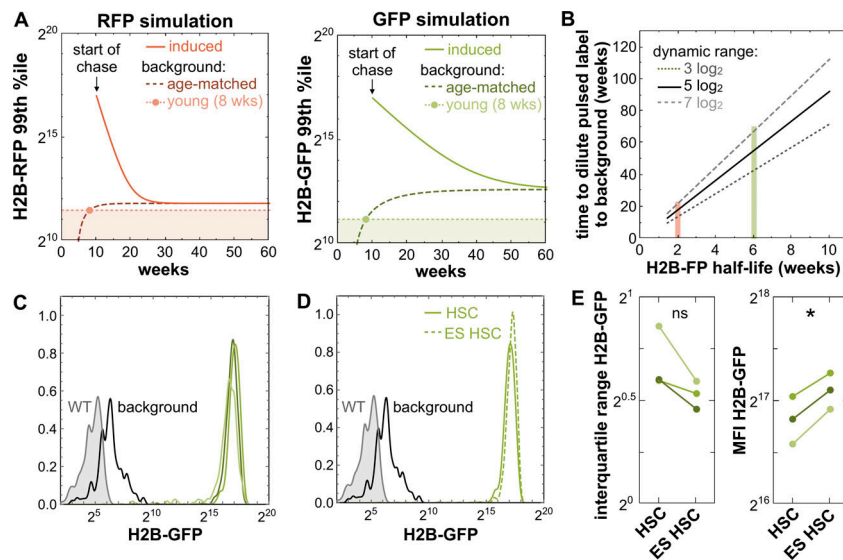


Figure S3. **Mitotic activity of HSC populations inferred from H2B-FP label dilution data. (A and B)** Representative examples for mixtures of Gaussian distributions, which were fitted to H2B-RFP (A, data from [Morcos et al., 2017](#)) or H2B-GFP (B, data from experiment shown in [Fig. 2 A](#) “GFP Morcos”) pulse-chase data of HSCs (continuous line: recorded data; dotted gray: fitted mixture distributions). Two Gaussians (RFP<sup>lo</sup> and RFP<sup>hi</sup>) were fitted to H2B-RFP retention data (0–19 wk of chase), while for H2B-GFP data (0–21 wk of chase), two peaks (GFP<sup>lo</sup> and GFP<sup>hi</sup>) were initially observed, but starting from 14 wk, a third, intermediate peak uniformly appeared (GFP<sup>mid</sup>). **(C)** H2B-RFP dilution time course of fitted RFP<sup>lo</sup> (light red, open circles) and RFP<sup>hi</sup> (dark red, filled circles) Gaussian distributions from chased CD34<sup>-/lo</sup> HSCs (LSK CD48<sup>-/lo</sup>CD150<sup>+</sup>CD34<sup>-/lo</sup>, upper panel, individual mice from [Morcos et al., 2017](#)) is shown. Division rates (lower panel) and respective 95% confidence intervals (tinted area and square brackets) of RFP<sup>lo</sup> and RFP<sup>hi</sup> CD34<sup>-/lo</sup> HSCs were calculated.



**Figure S4. Dynamics of H2B-FP dilution experiments.** **(A)** Simulation depicts H2B-FP pulse-chase experiments using either H2B-RFP (left panel) or H2B-GFP (right panel) mouse models. Label decay in HSCs of pulsed and chased mice (continuous line) was calculated using our mathematical model. The age-dependent accumulation of background fluorescence in repressed control mice (dashed line) was additionally simulated. For the special case of a non-age-matched background control (young, light dotted line), we arbitrarily assumed 8 wk of a age, which equals to ~4 wk after HSCs have entered a predominantly quiescent state. Non-age-matched background controls result in under-estimation of the gating threshold for identification of H2B-FP<sup>+</sup> HSCs and a seemingly label-retaining HSC population. **(B)** Simulation reveals the maximum chase interval until pulsed label fluorescence completely merges with accumulating background fluorescence. Merging of the populations was defined as the point when background fluorescence intensity equals 95% of the fluorescence intensity of the chased population. This simulation was performed for three different arbitrary dynamic ranges (span between maximum pulse labeling and background fluorescence) and variable protein half-lives of the H2B-FP (half-life estimates for H2B-RFP and H2B-GFP are depicted in red and green, respectively). **(C–E)** *R26<sup>rtTA/rtTA</sup>/Col1A1<sup>H2B-GFP/H2B-GFP</sup>* mice ( $n = 3$ , shown in green) were DOX-induced (2 g DOX/kg chow ad libitum) for 3 wk. Un-induced *R26<sup>rtTA/rtTA</sup>/Col1A1<sup>H2B-GFP/H2B-GFP</sup>* (black line) and B6 (WT, tinted gray area) mice served as background and autofluorescence controls, respectively. **(C)** Homogeneity of H2B-GFP labeling in HSCs (LSK CD48<sup>-/lo</sup>CD150<sup>+</sup>) in three pulsed individuals is depicted. **(D)** H2B-GFP distributions of LSK CD48<sup>-/lo</sup>CD150<sup>+</sup> (HSC, continuous green line) and CD201<sup>hi</sup> LSK CD48<sup>-/lo</sup>CD150<sup>+</sup> (ES HSC, dashed green line) populations from a representative DOX-pulsed *R26<sup>rtTA/rtTA</sup>/Col1A1<sup>H2B-GFP/H2B-GFP</sup>* mouse were overlaid and exemplify similar labeling homogeneity of HSCs and the primitive ES HSC subpopulation. **(E)** Interquartile range (left plot) and median (right plot) of H2B-GFP fluorescence intensity of the total HSC population were compared with the respective ES HSC subpopulation of the same DOX-induced individual (connecting lines). The interquartile ranges (labeling span of average events) of HSCs and ES HSCs revealed similar labeling homogeneity, while ES HSCs exhibited slightly higher labeling than HSCs. \*,  $P = 0.01–0.05$ ; ns, not significant.

Table S1 is provided online and lists antibody conjugates used for flow cytometry.